TRIBHUVAN UNIVERSITY
INSTITUTE OF ENGINEERING
PULCHOWK CAMPUS

FABRICATION, STRUCTURAL INTEGRITY, AND DYNAMIC RESPONSE OF A CARBON FIBER WING WITH STUDY ON MATERIAL PROPERTIES AND VIBRATION CHARACTERIZATION

By:
Bikesh Shrestha (077/BAS/006)
Gaurav Jung Karki (077/BAS/010)
Manish Shrestha (077/BAS/022)
Utsav Parajuli (077/BAS/047)

A PROJECT THESIS SUBMITTED TO THE DEPARTMENT OF MECHANICAL AND AEROSPACE ENGINEERING IN PARTIAL FULFILLMENT OF THE REQUIREMENT FOR THE BACHELOR'S DEGREE IN AEROSPACE ENGINEERING

DEPARTMENT OF MECHANICAL AND AEROSPACE ENGINEERING
LALITPUR, NEPAL

MARCH,2025

COPYRIGHT

TRIBHUVAN UNIVERSITY

INSTITIUTE OF ENGINEERING

PULCHOWK CAMPUS

DEPARTMENT OF AEROSPACE AND MECHANICAL ENGINEERING

LETTER OF APPROVAL

The undersigned certify that they have read, and recommended to the Institute of Engineering for acceptance, a project report entitled **"FABRICATION, STRUCTURAL INTEGRITY, AND DYNAMIC RESPONSE OF A CARBON FIBER WING WITH STUDY ON MATERIAL PROPERTIES AND VIBRATION CHARACTERIZATION"** submitted by **Bikesh Shrestha, Gaurav Jung Karki, Manish Shrestha and Utsav Parajuli** in partial fulfillment of the requirements for the Bachelor's Degree in Aerospace Engineering.

Supervisor: **Assoc. Prof. Dr. Surya Prasad Adhikari,**
Associate Professor
Department of Mechanical and Aerospace Engineering
Institute of Engineering, Pulchowk Campus

External Examiner: **Er. Bibek Dhungana,**
Assistant Professor
Department of Automobile and Mechanical Engineering
Institute of Engineering, Thapathali Campus

Head of Department : **Sudip Bhattarai (PhD),**
Assistant Professor
Department of Mechanical and Aerospace Engineering
Institute of Engineering, Pulchowk Campus

DATE OF APPROVAL: March 10, 2025

ABSTRACT

This study focuses on the design, fabrication, and analysis of a carbon fiber composite wing for UAV applications, aiming to optimize strength, weight, and durability. Carbon fiber-reinforced polymer (CFRP) was selected for its superior strength-to-weight ratio, stiffness, and environmental resistance. The wing structure integrates an 8.5mm carbon fiber rod and a 2mm thick carbon fiber sheet using an epoxy-based layup technique. A comprehensive investigation was conducted on material properties (Young's modulus ranging from 1.17-23.96 GPa), wing vibrations, and deformation analysis, utilizing high-speed camera imaging and finite element analysis (FEA) to assess structural integrity under aerodynamic loads with limit load being 22.45 N. Experimental findings were validated against analytical and numerical models, providing insights into modal frequencies (first mode) , damping characteristics, and mechanical performance. Additionally, various molding techniques (foam molding, 3D-Printed Mold, hand layup, and wooden mold) were evaluated for cost-effectiveness and feasibility. The results contribute to the advancement of lightweight, high-performance UAV wings, offering valuable insights into CFRP fabrication, vibration mitigation, and structural optimization in aerospace engineering.

Keywords: UAV, Carbon Fiber Composite, Structural Integrity, Finite Element Analysis, Vibration Analysis, Wing Fabrication, Aeroelasticity

ACKNOWLEDGEMENT

First and foremost, we would like to express our sincere gratitude towards **Assoc. Prof. Dr. Surya Prasad Adhikari** , our project supervisor for his constant guidance, inspiring insights and precious encouragement. Without his invaluable supervision and suggestions, it would have been a difficult journey for us. His useful suggestions for this whole work and cooperative behaviour are sincerely acknowledged. We would also like to express our sincere gratitude to **Asst. Prof. Ashish Karki**, for his invaluable guidance, insightful suggestions, and support during the initial stages of our project. His lectures and advice greatly contributed to shaping the direction of our work.

We would like to thank the **Department of Mechanical and Aerospace Engineering, Institute of Engineering, Pulchowk Campus** for providing us opportunity of collaborative undertaking which has helped us to implement the knowledge gained over these years as major project for fourth year, and develop a major project of our own that has greatly enhanced our knowledge and provided us a new experience of teamwork.

We also extend our gratitude to **Er. Abhishek Bhandari** and **Er. Aayush Bhatta** for sharing their valuable knowledge on composite materials and providing essential guidance throughout the completion of the project. Insights from Project Coordinator **Asst. Prof. Biman Rimal** and **Asst. Prof. Arun Bikram Thapa** were invaluable for progress of this project. We would also like to thank **Hukum Group of Company Pvt. Ltd** for the industrial visit of mold making. Also, we are thankful to **IOE, Thapathali Campus** for UTM setup.

We would also like to thank all of our friends who have directly and indirectly helped us in doing this project. Last but not the least, we place a deep sense of appreciation to our family members who have been constant source of inspiration for us.

Any kind of suggestion or criticism will be highly appreciated and acknowledged.

Authors:
Bikesh Shrestha
Gaurav Jung Karki
Manish Shrestha
Utsav Parajuli

TABLE OF CONTENTS

List of Figures

List of Tables

LIST OF ABBREVIATIONS

UAV	Unmanned Aerial Vehicle
CFRP	Carbon Fiber Reinforced Polymer
FRP	Fiber Reinforced Polymer
UV	Ultra Violet
FE	Finite Element
CFD	Computational Fluid Dynamics
AOA	Angle Of Attack
FEA	Finite Element Analysis
CNC	Computer Numerical Control
PLA	Poly Lactic Acid
PAN	Polymerization of Acrylonitrile
CAD	Computer Aided Design
GSM	Grams Per Square Meter
DMF	Dimethylformamide
DMAC	Dimethylacetamide
DMSO	Dimethylsulfoxide
PPE	Personal Protective Equipment
VF	Volume Fractions
CFERCM	Carbon Fiber Epoxy Resin Composite Materials
AN	Acrylonitrile
TMDs	Tuned Mass Dampers
UTM	Universal Testing Machine
ASTM	American Society for Testing and Materials
PMMA	polymethyl methacrylate

LIST OF SYMBOLS

Al	Aluminum
E	Young's Modulus
I	Moment of Inertia
m	Mass per unit length
L	Length of wing
T	Titanium
s	Wing area
b	Wing span
n	Wing loading
c	Chord length
α	angle of attack
ρ	Air Density
C_l	Coefficient of Lift
$(VF)_{ct}$	Volume Fraction of Carbon Tube
$(VF)_{cf}$	Volume Fraction of Carbon Fiber Fabricated Part
$(VF)_{acry}$	Volume Fraction of Acrylic Support Part
E_{wing}	Young's Modulus of Wing
V_{skin}	Volume of Skin and ribs
E_{spar}	Young's Modulus of spar
V_{spar}	Volume of spars
E_{skin}	Young's Modulus of fabricated carbon fiber skin and ribs
E_{spar}	Young's Modulus of acrylic support part
V_{spar}	Volume of acrylic support part
V_t	Total Volume of Wing
V_{cf}	Volume of ribs and skin
V_{ct}	Volume of carbon tube
M_{cf}	Mass of ribs and skin
ρ_{cf}	Density of Fabricated part
rho_{ct}	Density of carbon tube
ρ_{acry}	Density of PMMA acrylic support part
A_{spar}	Cross-sectional Area of Carbon Tube
R_{outer}	Outer radius of Carbon tube
R_{inner}	Inner radius of Carbon tube
ΔL	Change in length
σ	Stress
ε	Strain
$\beta_n L$	Frequency parameter

1. INTRODUCTION

1.1. Background

Unmanned Aerial Vehicles (UAVs) have become an essential component of modern aviation, with applications ranging from military surveillance and aerial mapping to agriculture and logistics. Among the critical structural components of a UAV, the wing plays a vital role in determining its aerodynamic efficiency, stability, and overall performance. Recent advancements in manufacturing techniques and material science have significantly enhanced UAV performance by enabling the development of durable and lightweight structures. This has been achieved through the use of advanced composite materials, which offer high strength, ballistic resistance, and rigidity.

The research aims to develop a lightweight yet robust wing, leveraging the superior strength-to-weight ratio and durability of carbon fiber composites to enhance aerodynamic efficiency and structural performance. Wing development for unmanned aerial vehicles (UAVs) is a multi-stage work such as airfoil selection, geometric calculation, structural design, material selection, numerical analysis, and manufacturing [2]. The primary goal of wing development is to create a structure that combines high strength with minimal weight. In alignment with this objective, carbon fiber—a widely recognized lightweight fiber-reinforced polymer—stands out as an optimal material for wing design due to its exceptional strength-to-weight ratio and durability.The internal frame of the wing incorporates an 8.5mm diameter carbon fiber rod and a 2mm thick carbon fiber sheet, hand-laid with epoxy and hardener. The selection of these materials ensures structural integrity while allowing for ease of fabrication, enabling quick design modifications and efficient prototyping. Additionally, the carbon fiber rod plays a crucial role in absorbing and distributing stress, thereby enhancing the wing's resilience. Its natural vibration-damping properties further contribute to smoother flight performance by mitigating the impact of minor turbulence.

1.2. Problem Statement

The use of carbon fiber-reinforced polymer (CFRP) composites has become increasingly prevalent in the aerospace and automotive industries, particularly for applications requiring low production volumes and high-value components. In aerospace, CFRP composites are extensively used to manufacture various parts, offering numerous benefits such as weight reduction, corrosion resistance, enhanced aerodynamic efficiency, customization, and design

flexibility. These advantages have driven the growing demand for advanced composite materials in the aerospace sector. Despite the increasing potential for CFRP composites, the fabrication processes in Nepal are still in the early stages of development. With the growing interest in composite materials, there is an opportunity to innovate and establish effective, locally accessible solutions for the production and fabrication of high-quality composite parts.

This project focuses on the initial development of a CFRP composite wing model, aiming to contribute to the advancement of local composite manufacturing techniques. To optimize the molding process, affordable wood molds have been used, providing a fine finish suitable for the fabrication of parts. Additionally, UV curing techniques are being explored as a means to further enhance the surface quality of composite parts, which may become a key part of the fabrication process in the future. The project's goal is to lay the foundation for the development and fabrication of composite components for aerospace purposes, with the potential to expand the use of CFRP composites in Nepal's aerospace industry.

1.3. Objectives

1.3.1. Main Objective

1. The primary objective of this project is to design, fabricate, and conduct a comprehensive vibrational analysis of an unmanned aerial vehicle (UAV) wing that utilizes advanced carbon fiber composite materials on the skin and wing frame structure.

1.3.2. Specific Objectives

1. To fabricate the carbon fiber composite skin, fabricate the frame structure and assemble the prototype using various molding technique.
2. To analyze the wing geometry with proper meshing.
3. To make account for molding process of different shapes optimizing quality.
4. To study the deflection and vibration of wing using high-speed camera to understand its dynamic behaviour.
5. To study material properties under microscope and Universal Testing Machine (UTM).

1.4. Carbon Fiber

There are many materials/material groups that are purely present in the nature and produced. These existing materials are classified according to their structures and utilized according to the place of usage. CFRP composite materials, from the advanced composite material class, are commonly preferred in strategic applications due to their outstanding features such as high load carrying capacity and low density. In many types of composites, FRPs count among the most high-performance materials in the field of light-weight design While the reinforcing elements of the composite material may be of different types (glass, carbon, aramid, etc.), the matrix materials are generally metal, ceramic or plastic. Composites composed of matrix and reinforcing components contain reinforcing fibers in a matrix resin[4].

- are microscopically homogeneous
- have major differences in the mechanical properties of component materials
- have volumetric ratio of the component materials greater than 10
- should improve performance.

The use of composite materials in the field of aerospace industry is increasing day by day. Its distinct anisotropic, heterogeneous structure and non-deformable properties make composite materials more prominent compared to other metallic materials. When composite materials are compared with other conventional materials, it is seen that these materials are particularly superior in their elasticity/density and strength/density ratios. Moreover, properties such as weight, abrasion resistance, fatigue life, corrosion resistance, stiffness, strength, heat insulation can be improved with composite material structures. The performance of the systems in aerospace industry is significantly influenced by innovations in materials and design approaches.

1.5. Measuring the Vibration Response of a Wing Using a High-Speed Camera

1.5.1. Advantages of High-Speed Cameras in Vibration Analysis

Data collection systems that employ high-speed cameras have become a cornerstone in experimental vibration analysis, particularly in aerospace applications. By capturing high-resolution temporal and spatial data, this technique facilitates accurate vibration analysis and improves the understanding of wing dynamics under varying conditions.

High-speed cameras are highly effective for capturing rapid and complex motion, making them ideal for vibration response measurements. A camera clocked at high fps can record minute oscillations that occur in milliseconds, providing a detailed visualization of the wing's motion. The non-contact nature of this technique eliminates interference with the wing's dynamics, a common issue in traditional contact-based methods like accelerometers. Furthermore, the high spatial resolution of high-speed cameras enables the measurement of localized deformation and modal shapes, which are critical for understanding structural behavior under aerodynamic loads.

The use of high-speed cameras operating at 1000 frames per second (fps) has proven highly effective in capturing the real-time deformation of composite aircraft wings. This approach demonstrates unparalleled accuracy compared to conventional sensor systems, thereby affirming the reliability of high-speed imaging technology in dynamic structural analysis.

1.5.2. Vibration Monitoring and Analysis Techniques

Monitoring the vibration of aircraft wings is critical to ensuring their operational safety and performance. High-speed cameras provide an innovative platform for such analysis, enabling real-time tracking of dynamic structural behaviors. The high frame rate allows for the detection of subtle harmonic distortions and transient oscillations that traditional sensors might miss. For example, transient vibrations caused by gust loads or rapid maneuvering can be analyzed with high-speed imaging to identify potential stress points.

A crucial aspect of vibration monitoring involves the detection of resonant frequencies. High-speed cameras can effectively capture these frequencies, facilitating the identification of operational conditions that might induce fatigue or structural damage. The detailed visual data obtained through this process can be coupled with finite element models to predict long-term durability and performance under various flight conditions.

1.5.3. Wing Load Deformation Data Collection

In addition to vibration monitoring, high-speed cameras are instrumental in collecting data on wing load deformation. During flight, aerodynamic forces exert significant loads on the wing structure, causing it to bend, twist, or deform. High speed cameras can capture these deformations in real-time, providing invaluable insights into the wing's aerodynamic and structural performance.

1.5.4. Role in Aero-elastic Studies

Aeroelasticity, the study of interactions between aerodynamic forces and structural dynamics, is a key area where high-speed cameras are utilized. Flutter, a dangerous oscillatory instability, is a critical aeroelastic phenomenon that can lead to catastrophic structural failure if not properly understood and mitigated. High-speed cameras are used to capture the rapid oscillations associated with flutter, providing precise measurements of amplitude, frequency, and damping ratios.

For instance, in wind tunnel tests, high-speed cameras record the wing's response to varying flow conditions. The resulting data is used to calibrate computational aeroelastic models, improving their predictive accuracy. Such studies ensure that aircraft are designed to operate safely within defined flight envelopes.

1.5.5. Challenges in High-Speed Camera Data Collection

Despite their advantages, high-speed cameras face challenges in data collection for vibration and deformation analysis. The sheer volume of data generated at high frame rates requires robust storage solutions and efficient processing algorithms. Environmental factors such as vibration of the camera setup, inadequate lighting, or reflective interference can impact data quality.

1.6. Microscopic Assessment in Material Analysis

Microscopic assessment is a fundamental technique in material science and structural analysis, facilitating the evaluation of micro structural characteristics, defect identification, and material deformation behavior. Microscopic analysis provides a quantitative and qualitative understanding of grain structure, phase distribution, surface morphology, and defect propagation, which are essential for assessing material integrity.

Advanced imaging techniques such as optical microscopy, scanning electron microscopy (SEM), and high-speed imaging are commonly used to capture high-resolution images of material surfaces and internal structures. These images serve as primary datasets for further analysis using computational tools and image processing techniques.

1.7. Feasibility

1.7.1. Economic Feasibility

The total cost of the project is completed at Rs.41000. The formation of composite lab also helped to cover the cost of this project, making it economically feasible. Furthermore, the fabrication process demonstrated the potential for scaling up to meet future demands in the aerospace industry, with the opportunity for local industries to adopt similar methods for composite part production.

1.7.2. Technical Feasibility

Technically, the project utilized proven composite fabrication techniques, including carbon fiber-reinforced polymer (CFRP) composites and wood molds, alongside SOLIDWORKS for precise design modeling and ANSYS for structural analysis, ensuring strength and reliability. The successful implementation of UV curing enhanced the surface finish and strength of the composite parts, demonstrating the potential for further innovations in local composite manufacturing.

The project successfully laid the groundwork for the future development of composite fabrication techniques for aerospace applications, with the use of advanced simulation and analysis tools ensuring that the final design met the required engineering standards.

1.8. System Requirements

To successfully carry out the project, the following hardware and software requirements were essential to meet the design, fabrication, and analysis needs:

1.8.1. Hardware Requirements

- Laser cutter
- CNC Foam Cutter
- 3D Printer
- UV Lamp

- High Speed Camera (Cronos 1.4)
- Digital Microscope (Leica DM750)

1.8.2. Software Requirements

- ANSYS
- MATLAB
- SOLIDWORKS
- RD Works
- XFLR5
- CaptaVision

2. LITERATURE REVIEW

2.1. Ribs Design

The maximum deformation of wing rib without cut- outs is less compared to that of wing rib with circular cut-outs. Moreover, the stress in wing rib without cut-outs is less than the wing rib with circular cut-outs. The mass of wing rib with circular cut-outs is lesser than the mass of wing rib without cut-out.

Carbon epoxy has more strength to weight ratio compared to that of Aluminium 7075-T6. So instead of metallic alloys like Al 7075-T6 we can also use carbon epoxy[5].

2.2. Epoxy

Among the carbon fiber composites, one material has become an important structural material in the aerospace field, which is carbon fiber epoxy resin composite material (CFERCM). Carbon fiber is a novel form of fiber material, which contains more than 90% carbon. It has high modulus, high strength and excellent comprehensive performance. A type of polymer known as epoxy resin is any polymer with more than two epoxy groups in its molecular structure. The composite of carbon fiber reinforced material and epoxy resin matrix is called carbon fiber epoxy resin composite material.

Carbon fiber can be utilized as both a load-bearing structural material and a functional material, so the development of carbon fiber and its composite materials is very rapid in recent ten years at home and abroad. Epoxy resin has the characteristics of high mechanical properties, small curing shrinkage, good technology, good bonding performance, great stability and so on. Carbon fiber and epoxy resin complement each other, making CFERCM have many good properties[6].

Epoxy resin has been of significant importance to the engineering community for many years. Components made of epoxy-based materials have provided outstanding mechanical, thermal, and electrical properties. Using an additional phase (e.g. inorganic fillers) to improve the properties of epoxy resins has become a common practice. It has been established in recent years that the polymer based composites reinforced with carbon fiber can significantly improve the mechanical, thermal, and barrier properties of the pure polymer matrix. Moreover, these improvements are achieved through conventional processing techniques without any detrimental effects on processability, appearance, density, and ageing

performance of the polymer matrix. Due to the above characteristics, the laminated fiber-reinforced composite materials such as epoxy/carbon fiber composites are widely applied in packaging, coating, electronics, automotive, and aerospace industries. They have high strength-to weight and stiffness-to-weight ratios. These composites have unique advantages over monolithic materials, such as high strength, high stiffness, long fatigue life, low density, corrosion resistance, wear resistance, and environmental stability. Laminated composites are susceptible to mechanical damages when they are subjected to efforts of tension, flexural, and impact, which can lead to material failure. Therefore, it is necessary to use materials with improved mechanical properties. Mechanical properties of epoxy polymeric composites can be enhanced through the improvement of the interlaminar properties by toughening resin matrix and fiber reinforcement. Rahmani et al.investigated the influence of fiber orientation, fiber content, and number of plies on mechanical prosperities. When composite materials are designed, the reinforcements are always oriented in the load direction. However, if the load direction is variable and not parallel to the fibers, it becomes more important to investigate the laminate mechanical behavior[7].

To meet the design requirements of the damage tolerance of the aircraft, the composite bearing structure of the composite material adopts the composite material with high performance carbon fiber as the reinforcement and high temperature curing high toughness epoxy resin.Carbon fiber reinforced epoxy resin matrix composite material is carbon fiber reinforced, epoxy resin as the matrix. As the carbon fiber is a brittle material, it can be compounded with epoxy resin to improve the toughness of composite materials, and carbon fiber excellent mechanical properties can also give the composite good strength and stiffness. In the process of preparing the carbon fiber reinforced epoxy resin composite material, the carbon fiber and the epoxy resin matrix are preliminarily prepared by prepreg, and then the prepreg is made into composite material by the molding process[8].

Epoxy Resins: Epoxy Resins exist either as liquids with lower viscosity or as solids. Compared to other materials, epoxy resins have several unique chemical and physical properties. Epoxy resins can be produced to have excellent chemical resistance, excellent adhesion, good heat and electrical resistance, low shrinkage, and good mechanical properties, such as high strength and toughness. These desirable properties result in epoxy resins having wide markets in industry, packaging, aerospace, construction, etc. They have found remarkable applications as bonding and adhesives, protective coatings, electrical laminates, apparel finishes, fiber-reinforced plastics, flooring and paving, and composite pipes[9].

Curing agents (Hardeners): Pure epoxy resin is only a thermoplastic low molecular weight prepolymer, not much use value, so the need to join the curing agent to form a three-dimensional epoxy resin network structure to play its maximum use. Epoxy resin vari-

ety, different types have different curing temperature, generally divided into: low temperature curing (room temperature below), room temperature curing (room temperature 50 °C), medium temperature curing (50 - 130 °C) and high temperature curing (130 °C the above). Low temperature curing has always been pro-gaze, mainly because it can greatly reduce the cost of output, compared to low-temperature curing, high-temperature curing of the equipment will certainly put stringent requirements, but can get excellent heat resistance curing products. Therefore, it is necessary to select the appropriate curing agent according to the curing temperature of the epoxy resin to fully reflect the effect of the curing agent, while giving the best performance of the cured product. The most widely used curing agents are mainly polyamine and acid anhydride type, because they can provide very active groups, only a small amount of the need to participate in the system curing and curing the system completely, they are able to Directly through the addition principle directly involved in the entire process of curing to go. Curing agents play an important role in the curing process of epoxy resin because they relate to the curing kinetics, reaction rate, gel time, degree of cure, viscosity, curing cycle, and the final properties of the cured products[9].

The effect of hardener on mechanical properties of carbon reinforced phenolic resin composites for hardener contents ranging from (5-15) wt.%, then composites with 15% hardener content show an increase in flexural strength, tensile strength and hardness. Among thermosett polymers, epoxy resins are the most common matrices for high performance aramid-fiber composites due to their easy processing[10].

Selection of Curing Agents: The selection of curing agents is a critical parameter. There are numerous types of chemical reagents that can react with epoxy resins. Besides affecting viscosity and reactivity of the formulation, curing agents determine both the types of chemical bonds formed and the functionality of the cross-link junctions that are formed. Thermal stability is affected by the structure of the hardener[9].

Prepreg: The prepreg is a prepreg product which is made of resin impregnated with resin and is an intermediate product of composite material. Depending on the properties of the desired composite material and the intended use, there are various differences in the preparation of the prepreg. Wet preparation of prepreg, not only easy to operate, simple equipment, but also has the characteristics of versatility, most of the prepreg can be prepared by wet method, but due to wet preparation process to enhance the proportion of fiber and resin Difficult to control, it is difficult to prepare uniform performance of the prepreg, and thus affect the overall performance of composite materials. Compared with the wet method, dry method can be a good way to overcome the shortcomings of the wet method, while the dry method can also avoid the volatile content of the wet, further control the performance of the prepreg to optimize. Whether it is wet or dry or dry and wet method, are more suitable for

thermosetting prepreg, for thermoplastic prepreg, the main use of powder, such as powder electrostatic powder and powder suspension[8].

Thermo-mechanical behaviour of epoxy composite

Thermoplastic and thermosetting resins have their unique properties but generally thermosetting resins are preferred to mix with glass, carbon and Kevlar due to their higher strength and easily curing properties at room temperature. Thermosetting polymers are insoluble and infusible after cure because the chains are rigidly joined with strong covalent bonds. Epoxy is the most popular among the available thermosetting polymers due to its high strength, low viscosity, low volatility and lower shrinkage rates over other thermosetting polymers [2, 3]. Among thermoset polymers, epoxy resins are the most common matrices for high performance aramid fiber composites due to their easy processing[11].

Epoxy polymer composites with carbon fiber as reinforcement have an extensive range of applications in many industrial fields as: wind turbines, construction, aeronautics and aerospace due to their favorable strength-to-weight and stiffness-to-weight ratios , as well as their high thermal stability and excellent corrosion resistance. The performance of fiber-reinforced composites is affected by the properties of the constituent materials and the load transfer capacity from the matrix to the reinforcement, this latter feature determined by the interfacial chemical interactions between fiber and matrix. However, since the present interactions are poor due to the surface inertness of carbon fiber, the efficiency of composite is limited[12].

For composite manufacturing a suitable resin either thermoplastic or thermosetting is needed to blend with. Thermoplastic and thermosetting resins have their unique properties but generally thermosetting resins are preferred to mix with glass, carbon and Kevlar due to their higher strength and easily curing properties at room temperature. Thermosetting polymers are insoluble and infusible after cure because the chains are rigidly joined with strong covalent bonds. Typical examples of thermoset include epoxies, polyesters, phenolics and polyamide[1].

Effect of fiber loading on tensile strength of bi-directional carbon-epoxy composites

Figure 2.1 shows the plotted graph showing change in values of tensile strength with the change in percentage by weight of fiber composition. The tensile strength increases with the increase in fiber loading. An exceptional decrease in tensile strength values is noticed at 40wt. composition. This decrease may be due to improper bonding in between the matrix (epoxy) and the layer of carbon fiber and hence shear stress induced in between the layers of the composite. In chopped CFRE composites lower values of tensile strength are observed than that of bidirectional CFRE composites. This is due to the proper orientation

of fibers, loads can effectively be transferred from one end to another resulting in increased tensile strength whereas in chopped fibers, length of fibers are less (5-8) mm which cannot effectively transfer the stresses from one end to another resulting in lower values of tensile strength.[1]

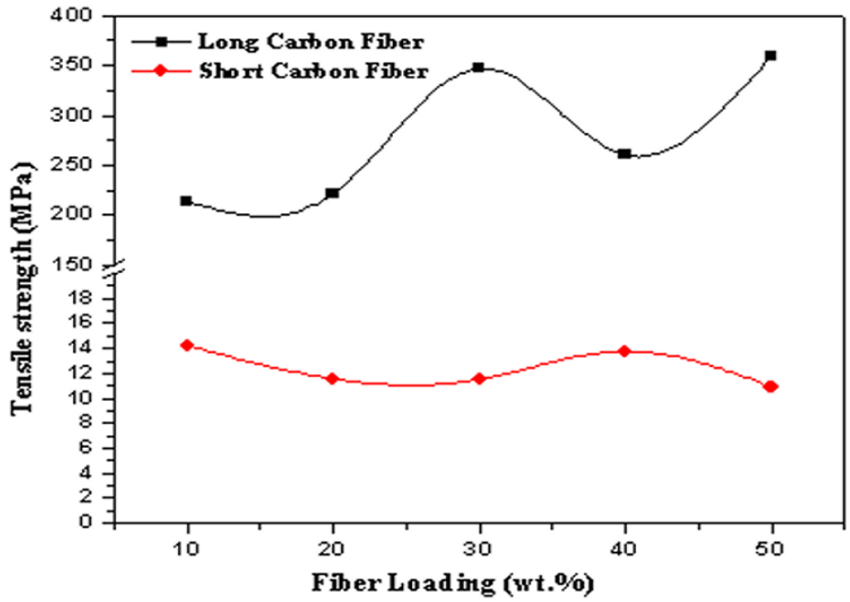

Figure 2.1: Effect of Fiber Loading on Tensile Strength of Long and Short CFRE Composites [1]

Tensile Strength

Carbon fibers are characterized by excellent tensile strength 2.4 – 3.1 GPa, elastic modulus 200 – 280 GPa and significant high temperature resistance (in an inert atmosphere, the mechanical properties do not change to 1500 °C)[13]. They are anisotropic materials with varying properties according to direction of layup.

Properties

Carbon fibers have low density, high strength and high stiffness properties. These fibers are usually 80-95 carbon-containing, can be in staple or filament form, have very good mechanical properties, and at the same time, they are lightweight and have density of 2268g/cm^3. CFRP have high specific strength up to 4500 MPa. They can withstand temperatures up to 3000°C. With retaining their structural integrity. CFRP has extremely high tensile strength/weight ratios, tensile modulus/weight ratios and high fatigue strength [4].

2.3. Carbon Fiber Reinforced Polymer (CFRP) Composite Materials

Carbon Fiber Reinforced Polymer (CFRP) is a composite material made up of carbon Fibers and a polymer resin, usually epoxy. The carbon Fibers provide the strength and stiffness, while the polymer resin acts as a binder that holds the Fibers together. This combination of materials results in a high-strength, lightweight material that is ideal for many applications. CFRP has several properties that make it a popular choice in many industries. It is lightweight, strong, stiff, and corrosion-resistant. It has a high strength-to-weight ratio, which means it can withstand high loads and stresses without adding unnecessary weight. It is also durable and can withstand harsh environments. Carbon fiber reinforced composite materials offer greater rigidity and strength than any other composites, but are much more expensive than e.g. glass fiber reinforced composite materials. Composites made from carbon fiber are five times stronger than grade steel for structural parts, yet are still five times lighter. In comparison to aluminum, carbon fiber composites are seven times stronger and two times stiffer, yet 1.5 times lighter[13].

Epoxy resins have been successfully used in composite applications since the 1960s. Epoxy resins are a class of thermoset materials used extensively in structural and specialty composite applications because they offer a unique combination of properties that are unattainable with other thermoset resins.

2.3.1. Carbon Fiber Fabrics

Carbon fiber (CF) fabric, once a specialized material reserved for the aeronautics and aerospace industries, is now regularly encountered in daily life. Commercially, it is valued for its lustrous good looks and has been embraced by architects as well as designers of furniture and decorative arts. Carbon fiber composites (CFCs) are becoming more common in sporting equipment and have been adopted by the sailing industry, in which carbon fiber is used in the fabrication of hulls, booms, masts, and even the sails themselves. One of the advantages of carbon fiber composites is that they can be fabricated in virtually any shape or size.

Carbon fiber fabric is a woven cloth made up of thousands of filaments; each filament is composed of primarily carbon atoms that are more or less aligned along the axis of the fiber. It is important to note here that the terms “graphite fiber” and “carbon fiber” are often used interchangeably, but this is a misuse of the terms. “Graphite” refers to a material with a specific molecular structure in which sheets of aromatic carbon atoms are regularly stacked so that they overlap with a carbon atom at the center of each ring. The most commonly available carbon fibers are rarely produced with a graphitic structural alignment. True graphite fibers,

which are produced for highly specialized purposes, universally have mechanical characteristics that far exceed those of standard carbon fiber, hence the importance of using the correct terminology when discussing these materials [14].

2.3.2. Material Characteristics of Carbon Fiber

The result of the thermal conversion process is a carbon filament ranging from 5 to 10 μm in diameter— a fraction of the thickness of a human hair. This tiny fiber has extraordinary characteristics. While the mechanical properties of CF can vary based on manufacturer, precursor, and specific manufacturing techniques, carbon fiber can be described generally as having a stiffness-to-weight ratio that makes it twice as stiff and five times stronger than steel [15].

Such strength comparisons are commonly reported, but describing carbon fibers in general terms in relation to steel may be misleading. The typical material characteristics used to describe the strength of carbon fiber are tensile strength, a measure of the pulling force a fiber can withstand before it fails, and Young's (or elastic) modulus, which measures the stiffness of a material, or its ability to resist elongation under load. Carbon fibers can be manufactured with a range of tensile strength and moduli. For example, it is possible to create a fiber with high tensile strength and low modulus. A low modulus would be necessary when flexibility is needed, while high modulus would be sought when bending or deflection is not desired[16]. For these reasons, it is inaccurate to make broad characterizations stating that CF is "n" orders of magnitude stronger than steel. It is more accurate to say that most CFs match or beat the strength and stiffness of steel.

Strength aside, one of the most desirable features of carbon fiber is its high strength-to-weight ratio. Carbon fibers are universally significantly lighter than steel, making them appropriate for a wide variety of applications for which low weight is required. Carbon fiber is also chemically resistant and does not corrode the way metals do. It has high temperature tolerance and a low coefficient of thermal expansion, making CF ideal for the construction of spacecraft. Carbon fibers are not subject to creep or fatigue failure, as metals are.

2.3.3. Fabric

Carbon Fiber tape is not adhesive backed but is called "tape" because it is woven to width with a selvage to prevent unravelling, one of the inconveniences of slippery carbon Fibers. The tape format is convenient if a project requires many narrow strips of fabric. When

layering with a laminating epoxy, the plain weave tape wets out quickly and handles easily. Only three layers are typically necessary to produce useful non-structural pieces, and it is particularly convenient for joining prefabricated parts together [17].

Pre-fabricated components are a convenient option for building structures that have regular geometries, as they are available in a wide variety of shapes, such as right angles, C channel, I beam, round or square tubes, and rods. These structural components can be cut with a band saw and then assembled using carbon Fiber tape and epoxy.

2.3.4. Resins

The three most commonly available laminating resins are polyester, vinyl ester, and epoxy. Polyester is widely used in the composite industry because it is less expensive and more forgiving than epoxy; it is typically paired with fiberglass fabric. Vinyl esters are low-viscosity resins and are well suited for vacuum infusion of composites. Despite the conveniences of other resins, epoxy is the best option for conservation projects because it outperforms polyester and vinyl ester resins in strength and dimensional stability. Epoxy is the most expensive resin of the three options. For the best results, conservators should always use the laminating resin recommended by their CF vendor. For example, when using FibreGlast's fabrics, best results will be achieved when using their FibreGlast 2000 epoxy system specifically designed for laminating CF fabric [17].

2.3.5. Types Of Carbon Fiber

1. PAN based Carbon Fiber: The polymerization of acrylonitrile (AN) is a critical step in producing PAN-based carbon fibers. Common methods include solution and suspension polymerization, with solution polymerization using solvents like DMAc, DMF, and DMSO, achieving high molecular weight copolymers but with lower conversion efficiency (50–70%) compared to suspension polymerization (90%). Wet spinning is the preferred method for fiber spinning due to PAN's high melting point, requiring solvents and a coagulation bath for fiber formation. Post-spinning processes include washing, drawing, and drying to enhance fiber properties. Stabilization occurs via oxidation at 200–300 °C, increasing fiber density, while carbonization at 200–1000 °C in an inert atmosphere converts PAN fibers into carbon fibers with 95% carbon content. Higher temperatures (2000 °C) yield graphite fibers. Surface treatment further enhances tensile strength and composite adhesion, making PAN-based carbon fibers ideal for high performance applications [18].

Properties

i. **High Tensile Strength:** The most prominent feature, though reduced by defects formed during synthesis.

ii. **Defects in Material:** Tensile strength is affected by defects caused by the weight loss (50%) of PAN during conversion to carbon fiber.

iii. **Surface vs. Internal Defects:** Surface defects (from oxidation, carbonization, or thermal processes) have a greater impact on tensile strength than internal defects.

iv. **Thermal Conductivity:** Can be enhanced by grafting carbon nanotubes onto the fiber, leveraging their high thermal conductivity.

2. Pitch Based Carbon Fiber: Pitch-based carbon fiber synthesis involves similar processes for isotropic and anisotropic pitch sources, derived from raw materials like aromatic compounds, petroleum by-products, or polyaromatic hydrocarbons. Impurities are removed using methods such as distillation, extraction, or centrifugation, and the pitch is prepared under controlled conditions of temperature, pressure, and mixing. The pitch is melt-spun into fibers in an inert atmosphere, followed by stabilization through oxidation to transition from thermoplastic to thermoset, ensuring structural integrity during carbonization. During carbonization (300–1400 °C), non-carbon atoms are removed, increasing aromaticity and forming the precise mechanical, physical, and chemical properties of the carbon fiber.

Properties

i. **Types:** Divided into isotropic and anisotropic (mesophase) types.

ii. **Anisotropy vs. Isotropy:**

- **Anisotropic (Mesophase):** Properties vary with direction, consisting of planarly stacked aromatic hydrocarbons and exhibiting optical anisotropy.
- **Isotropic:** Homogeneous properties in all directions.

iii. **Material Composition:** Mesophase pitch is a liquid crystal material composed of aromatic hydrocarbons.

iv. **Tensile Strength:**

- **Mesophase:** Up to 4 GPa.
- **Isotropic:** Lower, around 500–1000 MPa.

v. **Thermal Conductivity:** Mesophase pitch-based fibers have high thermal conductivity (1000 W/mK).

vi. **Density:** Mesophase fibers have a density of approximately 2 g/cm³.

vii. **Cost:** Isotropic pitch-based fibers are less expensive but offer reduced performance compared to anisotropic types.

3. Carbon Fiber Composites: Discovered in 1960, carbon fiber composites are widely used in automotive, aerospace, civil, mechanical engineering, shipbuilding, and wind turbine applications due to their durability, lightweight, and cost-effectiveness. These composites, often paired with thermoset matrices like epoxy or thermoplastic matrices such as polyethersulfone (PES), polyphenyl sulfide (PPS), polyetherimide (PEI), and polyimide (PI), enhance the thermal, mechanical, and electrical properties of polymers. Strengthening the physicochemical interactions between carbon fibers and polymers, primarily through Van der Waals and hydrogen bonds, is a focus of ongoing research. Production methods include extrusion, injection molding, and resin transfer molding. Recent studies explore moisture effects, surface functionality, and the use of carbon nanotubes to improve properties like conductivity and interface bonding.

Properties

i. **Composite Structure:** Made by combining two or more materials with distinct physical and chemical properties; consists of a soft, weak matrix embedded in a strong, hard support material to create a lightweight, mechanically strong material.

ii. **Surface Characteristics:** Carbon fiber has a smooth, chemically inert, and non-polar surface, requiring surface treatment to ensure good interfacial adhesion with the matrix.

iii. **Interfacial Bonds:** Adhesion is improved through Van der Waals forces, hydrogen bonds, or mechanical interlocking.

iv. **Interfacial Treatment Methods:**

- **Wet/Chemical Treatment:** Includes liquid-phase, electrochemical, or catalytic oxidation. Amine and carboxylic groups enhance adhesion after oxidation.
- **Dry Treatment:** Plasma surface modification.
- **Multi-Scale Approach:** Coating carbon fiber with materials like nanoparticles or carbon nanotubes to enhance strength, toughness, and resistance properties.

v. **Matrix Materials:**

- Thermoset polymers (e.g., epoxy, phenolic, polyimide).
- Thermoplastic polymers (e.g., ABS, polyamide, polyethylene).
- Carbon, metal (e.g., nickel), ceramic, and cement matrices.

vi. **Performance Factors:** Poor adhesion or interface material defects affect crack propagation, stress distribution, and overall performance.

4. Carbon Fiber-Carbon: Carbon fiber-carbon composites are synthesized using methods such as vacuum filtration, pressure filtration, dry synthesis, and powder molding. These materials are used as thermal insulators in NASA space vehicles and vacuum electric furnaces due to their ability to withstand up to 2800 °C in airless conditions. Other applications include gas adsorption, separation, and use as cathode materials in batteries. Despite their low density and high porosity, they have weak mechanical properties and are prone to oxidation, leading to recent advancements in coating technologies like aerogels and nanostructures for improved performance.

5. Carbon Fiber-Metal: Carbon fiber-metal composites combine carbon fibers with metallic matrices such as aluminum, titanium, magnesium, and nickel, among others, through processes like oxidative surface treatment and solid or liquid-state synthesis. These composites exhibit high mechanical resistance, excellent thermal and electrical properties, and low friction, making them ideal for aerospace, automotive, and petrochemical applications. Research continues to improve fiber distribution and mechanical properties using techniques like fuzzy logic and neural networks.

6. Carbon Fiber-Ceramic: Carbon fiber-ceramic composites, such as silicon carbide (SiC), are designed for aerospace applications due to their high-temperature resistance, toughness, and thermal shock resistance. They are particularly suited for rocket engines and are being enhanced for greater oxidation and mechanical strength at ultra high temperatures (above 3000 °C). Other ceramic matrices include ZrC, ZrB2, and SiC–TaC, with chemical vapor infiltration considered the most effective synthesis method.

7. Carbon Fiber-Concrete: Carbon fiber-reinforced concrete improves the mechanical, toughness, and durability properties of conventional concrete. High-performance concrete incorporates additives like silica fume and fly ash to increase compressive strength and durability. However, the brittleness introduced by these materials can lead to cracking, compromising water resistance and exposing the interior to moisture and corrosive agents. Researchers aim to balance the advantages of enhanced strength with solutions to mitigate cracking and its effects.

2.4. Curing

UV radiation is an electromagnetic radiation with wavelengths below those of visible blue light. While the energy of the radiation increases with decreasing wavelength, the depth of penetration into matter increases with the wavelength. With respect to the spectral absorption, ordinary glass is transparent to UV, but is opaque to shorter wavelengths of 350nm. Silica can be transparent to wavelengths down to 200 nm .Radiation at wavelengths smaller than 180 nm is strongly absorbed by the oxygen in air and by most common materials. Some polymer materials, such as polycarbonate, block most UV radiation. The intensity of UV radiation for continuous exposure is described by the irradiance which refers to the radiant energy flux or power incident on a surface, divided by the surface area. UV radiation is contained in the spectrum of natural sunlight or can be generated by various types of light sources[19]. As among the many components used in general acrylic monomers do not absorb UV-light in a very efficient way and will not initiate radical polymerization fast enough. As such, a photopolymer sable coating formulation essentially consists of a polymer sable vehicle and a light sensitive compound that is able to convert the absorbed light energy into more useful form capable of causing the binder to polymerize into a hard solid mass. Such a light sensitive compound is known as a photo initiator/ sensitizer. Thus, a photo initiator is added which produces initiator radicals either directly by the fragmentation of the photo-excited state, or in two steps, by hydrogen transfer from a suitable substrate to the photo-excited state [20].

Photo initiator is of paramount importance in radiation curable systems. A photo initiator is selective in terms of light of specific wavelengths. During formulation, the absorb characteristics of the photo initiator are matched to the radiation characteristics of the lamp output. Indeed, the choice of photo initiator is of prime importance in the light induced polymerization since it directly governs the cure rate. A suitable photo initiator system must first have a high absorption in the emission range of the light source, usually a medium pressure mercury lamp. In addition, the excited states thus formed must have both a short lifetime to avoid quenching by oxygen or the monomer, and split into reactive radicals or ionic species with the highest possible quantum yield. A photo initiator absorbs the incident light directly and split up or fragments to form free radicals. These then attack the monomer to initiate the photo polymerization reaction. In contrast, a photosensitizer absorbs the incident light but does not fragment itself, instead “transfers” the energy it has obtained to another compound (which may be the monomer), to procure initiation of the polymerization reaction. The selection of the photo initiator can be selected through various factor which can be listed down below [20]:

i. Required line speed with given curing system;

ii. The required coating thickness;

iii. Surface properties to be obtained such as hardness and gloss;

iv. Required non-toxic, low migration, and cost-effective properties;

v. Required high absorption in the region of the activation;

vi. Required high quantum yield for free radical formation.

Heating of the resin to reduce the viscosity during processing and to improve the impregnation of the reinforcement textile has no effect on the resin or the properties of the finished product. The ability to cure on demand allows laminates to be completely prepared in terms of fiber arrangement and impregnation prior to curing. Thus, the scrap rate is reduced. Since the resin does not gel on the molding equipment or in resin transfer lines, waste is reduced and there is no need for time-consuming and expensive cleaning operations.

2.5. Wing Vibrations

2.5.1. Introduction to Wing Vibrations

Aircraft wings are crucial yet susceptible components of an airplane, playing a key role in generating the necessary lift and drag forces. Constantly subjected to aerodynamic loads, ensuring their safety remains a top priority in the aviation sector. The wing's skin is securely fastened to all structural components and plays a crucial role in bearing a portion of the loads and stresses. During flight, the primary forces acting on the wing structure are absorbed by the skin, which then transfers these loads to the ribs and subsequently to the spars. The spars are responsible for carrying both distributed loads and concentrated weights, including the fuselage, landing gear, and nacelle[21]. The study of vibration characteristics in various airfoil wings has become increasingly important. A fundamental approach to understanding aeroelastic effects involves analyzing dynamic properties such as natural frequencies and mode shapes. This analysis helps in minimizing noise emissions and identifying vibration sources that may lead to structural damage. Implementing modal analysis enhances the system's overall performance[22].

Aircraft wings are continuously subjected to aerodynamic, structural, and inertial forces, making them prone to vibrations. These vibrations can arise due to various factors, such as airflow fluctuations, structural flexibility, and external disturbances. Understanding and

mitigating wing vibrations is crucial to ensuring flight safety, structural integrity, and aerodynamic efficiency.

2.5.2. Causes of Wing Vibrations

During flight conditions at high speed this wing of an aircraft is subjected to maximum lift forces over the top surface of the wing which will pave way for an increase in g-force and it starts to vibrate. This is a major factor that resist or reduces the stability of an aircraft.

Several factors contribute to the vibrations experienced by aircraft wings:

i. **Aeroelastic Effects:** The interaction between aerodynamic forces and structural elasticity leads to phenomena like flutter and divergence.

ii. **Turbulent Airflow:** Variations in airflow due to turbulence can induce oscillations in wing structures.

iii. **Engine and Propeller-Induced Vibrations:** Aircraft propulsion systems generate vibrational forces that can propagate through the airframe to the wings.

iv. **Structural Deformations:** Material properties, manufacturing imperfections, and fatigue can lead to vibrations due to changes in wing stiffness.

2.5.3. Types of Wing Vibrations

i. **Free Vibrations:** Occur when a system oscillates naturally without external forces after being disturbed. The frequency of these vibrations is determined by the wing's natural modes.

ii. **Forced Vibrations:** Result from continuous external excitations such as gust loads, engine operations, and atmospheric disturbances.

iii. **Flutter:** A self-excited, dynamic instability caused by aerodynamic and inertial coupling, potentially leading to catastrophic structural failure if uncontrolled. In the field of dynamic aeroelasticity, flutter stands out as one of the most extensively studied phenomena. It is regarded as a critical aspect of aeroelastic research and remains one of the most challenging effects to accurately predict. The aeroelastic behavior of an aircraft is determined by the interaction of its aerodynamic forces, structural characteristics, and mass distribution of its components.

iv. **Buffeting:** Irregular, high-intensity vibrations caused by turbulent airflow over the wing surfaces, often occurring at high speeds.

2.5.4. Analysis Methods for Wing Vibrations

Modal Analysis: Determines natural frequencies and mode shapes of the wing, helping in identifying resonance conditions. An aircraft wing can be modelled as a cantilever beam by neglecting all external forces acting on the aircraft, except for gravity. Modal analysis is a widely used technique for examining the dynamic behavior of mechanical structures under external excitations. It also plays a key role in minimizing noise transmission from the system to its surroundings[23].

Finite Element Method (FEM): Numerical simulations are performed to analyze the structural response of wings under dynamic loads. It allows for detailed modeling of complex geometries and material properties, providing insights into stress distribution, deformation, and natural vibration modes. By discretizing the wing structure into smaller finite elements, FEM enables accurate prediction of natural frequencies, mode shapes, and potential resonance conditions.

Computational Fluid Dynamics (CFD): Used to study aerodynamic loads and their impact on wing oscillations. Additionally, coupling FEM with Computational Fluid Dynamics (CFD) enhances the accuracy of aeroelastic simulations by incorporating aerodynamic forces acting on the wing.

Wind Tunnel Testing: Physical experiments conducted to observe wing behavior under controlled airflow conditions. These tests allow researchers to observe real-time aerodynamic interactions and structural deformations under controlled airflow conditions. Wind tunnel testing remains essential for aircraft certification and safety assessments, ensuring that wing structures perform optimally under real-world operating conditions.

Experimental Modal Analysis: Vibration measurements using accelerometers and laser vibrometers to validate numerical models. High-speed cameras, laser vibrometers, and pressure sensors are used to measure vibration amplitudes, flutter onset speeds, and buffeting effects. Additionally, scaled wing models with embedded strain gauges and accelerometers provide experimental data to refine computational models.

2.5.5. Wing Vibrations Mitigation Techniques

Structural Reinforcement: Using composite materials and optimized wing designs to enhance stiffness and reduce vibrations. The use of advanced composite materials, such as carbon fiber-reinforced polymers, improves rigidity while keeping the weight low. Additionally, techniques like rib and spar reinforcements, honeycomb structures, and optimized skin thickness distribution contribute to vibration reduction and increased durability.

Damping Mechanisms: Incorporation of passive and active damping systems, such as tuned mass dampers, to absorb excess vibrations. Passive methods, such as viscoelastic materials, tuned mass dampers (TMDs), and friction-based damping, absorb excessive energy from oscillations. On the other hand, active damping systems use sensors and actuators to dynamically counteract vibrations in real-time, improving overall stability and structural longevity.

Aeroelastic Tailoring: Designing wing structures with materials that adapt to aerodynamic loads, reducing the risk of flutter. The use of advanced composite materials in tailoring is a groundbreaking approach in the constantly evolving field of aerospace engineering. Aeroelastic flutter is a form of dynamic instability in flight vehicles, resulting from the interaction of aerodynamic, elastic, and inertial forces. This phenomenon leads to progressively increasing vibrations, which, if left uncontrolled, can ultimately cause severe structural failure. [24]

Active Control Systems: Implementation of smart actuators and sensors to counteract unwanted vibrations dynamically.

2.6. Analytical Methods for Wing Vibration Calculation

2.6.1. Wing Vibration Theory

The analysis of wing vibrations is crucial for understanding the dynamic behaviour of aircraft under various flight conditions. Accurate prediction of wing vibrations is essential not only for structural integrity but also for safety, comfort, and performance optimization. Analytical methods provide a foundational approach to calculating wing vibrations, offering insights into the natural frequencies, mode shapes, and responses to external excitations. To understand wing vibrations, it is necessary to model the wing structure as a dynamic system subjected to aerodynamic and inertial forces. Several classical theories and mathematical models are employed to derive the equations governing the vibration behavior of wings. These methods typically involve simplifying the complex geometry and boundary conditions of the wing into more manageable forms, such as beam models or plate structures,

which can then be analyzed using various dynamic principles.

The free vibration analysis of an aircraft wing is one of the most challenging aspects in aircraft design. A crucial factor in studying gust responses and aeroelastic phenomena is the analysis of natural frequencies and mode shapes. Aircraft wings are typically made of thin-walled, irregularly shaped structures, often incorporating sweep and dihedral angles, as well as tapering. These characteristics introduce complex effects that necessitate advanced structural modelling. There are three primary approaches for structural analysis of an aircraft wing: one-dimensional (beams), two-dimensional (plates, shells), and three-dimensional (solids). One key advantage of the one-dimensional model is its lower computational demand compared to the analysis of shells or solids. Well-known examples of classical beam models include Euler-Bernoulli and Timoshenko, with the latter accounting for transverse shear deformation and rotary inertia. As non-classical effects become more significant, the applicability of classical beam models diminishes due to their limitations [23].

2.6.2. Euler-Bernoulli Beam Theory

Euler-Bernoulli Beam Theory is a classical approach used to model the bending behavior of beams under load. In the context of wing vibration, it is often employed to simplify the analysis of the wing structure as a beam that can bend and twist under aerodynamic loads. The theory assumes that cross-sections of the beam remain perpendicular to the neutral axis during deformation, and it neglects the effects of shear deformation and rotary inertia.

When applied to wing vibrations, the Euler-Bernoulli theory helps in calculating the natural frequencies and mode shapes of the wing. The wing is typically modeled as a beam with specific boundary conditions, such as fixed, simply supported, or free ends. The wing's structural properties (like Young's modulus, moment of inertia, and mass distribution) are incorporated into the model to predict its dynamic response[25].

The natural frequency equations of Euler-Bernoulli Beam Theory are [3]:

$$\omega_n = (\beta_n L)^2 \sqrt{\frac{EI}{mL^4}} \tag{2.1}$$

Young's Modulus is denoted by E, the moment of inertia is denoted by I, unit mass is denoted by m, and length is denoted by L.

$$\frac{d^2}{dx^2}\left\{EI\frac{d^2Y(x)}{dx^2}\right\} = \omega^2 m(x)Y(x) \tag{2.2}$$

$$\beta^4 = \frac{\omega^2 m}{EI} \tag{2.3}$$

For different mode shapes ($n = 1, 2, 3, ...$), the value of $\beta_n L$ are calculated in Table 2.1 below:

N	$\beta_n L$
1	1.875
2	4.694
3	7.854

Table 2.1: Values of $\beta_n L$ for different mode shapes[3]

2.6.3. Calculations Of Bending Inertia

The vertical displacement of an aircraft wing can be determined by analysing the spanwise bending stiffness distribution along the primary load axis [2]. In this context, Young's Modulus acts as a scaling factor for the specific material used in the wing structure. The coordinates for the upper and lower surfaces of the wing are derived from the UIUC airfoil database, represented as $Y_u(x)$ and $Y_\ell(x)$, respectively. The total bending inertia is denoted by I, and A represents the cross-sectional area. As depicted in Figure 5, the model is subdivided into infinitesimally small quadrilateral units with a width of dx and a height corresponding to the difference between the upper and lower surfaces ($Y_u - Y_\ell$).

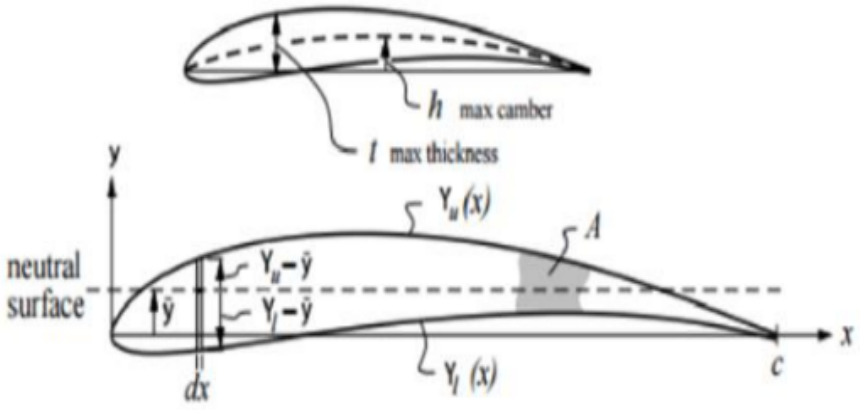

Figure 2.2: Parameters for determining bending inertia [2]

Equation 2.4 to equation 2.14 is adapted from [FinalG4] to calculate the bending inertia of the **airfoil** wing.

$$A = \int_0^c (Y_u - Y_\ell) dx \tag{2.4}$$

$$\bar{y} = \frac{1}{A} \int_0^c \frac{1}{2} (Y_u^2 - Y_\ell^2) dx \tag{2.5}$$

$$I = \int_0^c \frac{1}{3} [(Y_u - \bar{y})^3 - (Y_\ell - \bar{y})^3] dx \tag{2.6}$$

$$t = \max(Y_u(x) - Y_\ell(x)) \tag{2.7}$$

$$h = \max\left(\frac{(Y_u(x) - Y_\ell(x))}{2}\right) \tag{2.8}$$

$$\tau = \frac{t}{c} \tag{2.9}$$

$$\varepsilon = \frac{h}{c} \tag{2.10}$$

$$K_A = \frac{1}{c^2} \int_0^c A(Y_u(x) - Y_\ell(x)) dx \tag{2.11}$$

$$K_I = \frac{1}{c^4(\tau^2 + \varepsilon^2)} \int_0^c \frac{1}{3} [(Y_u - \bar{y})^3 - (Y_\ell - \bar{y})^3] dx \tag{2.12}$$

The typical values for K_I and K_A for the most commonly used **airfoils** are approximately 0.036 and 0.6, respectively. The moment of inertia, I, can be determined using the formulas provided in Eq. (2.13) and Eq. (2.14).

$$A = K_A c t \tag{2.13}$$

$$I = K_{tct}(t^2 + h^2) \tag{2.14}$$

2.6.4. Calculations of Clark Y Profiled Wing

The x-axis and y-axis coordinates can be sourced from the UIUC airfoil database and processed using Excel. The values for the x-axis are divided into Yu(x) and Yl(x), which correspond to the coordinates of the upper and lower surfaces of the airfoil, respectively. This method enables the accurate representation of the airfoil's shape for further analysis. The wing natural frequency is then calculated using Eq. (2.1).

3. METHODOLOGY

This chapter presents the project's methodology, organized into stages, with a detailed quantitative approach outlined in Figure 3.1, which illustrates the research development process.

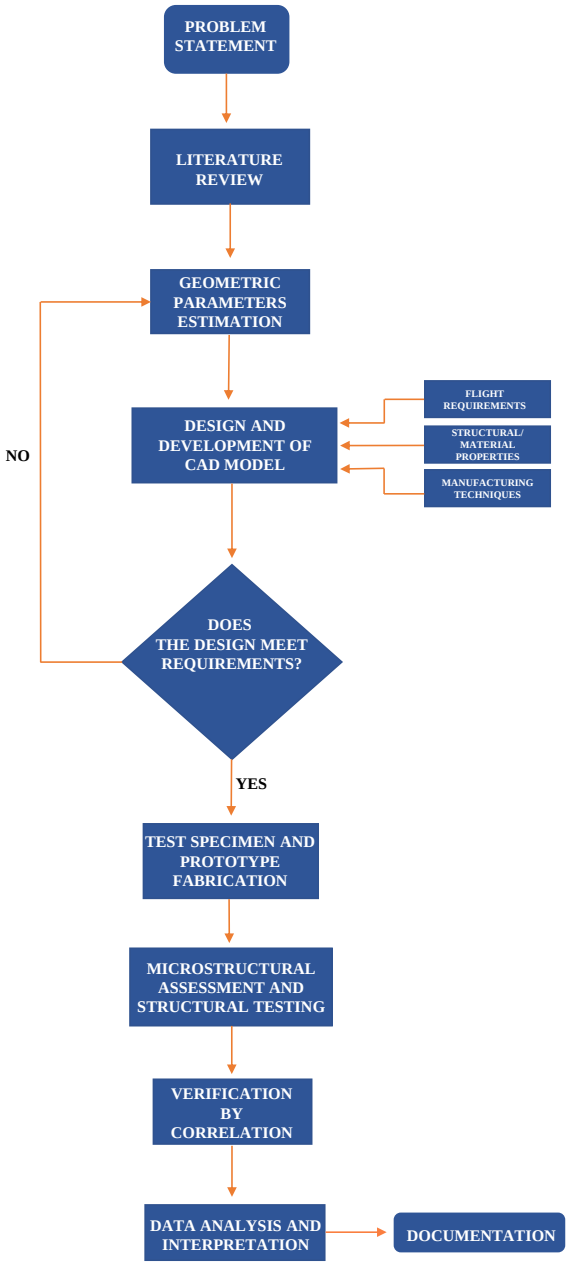

Figure 3.1: Methodology Flowchart

3.1. Wing Design

Designing of wing being an integral and foremost part of the project, selection of wing was done with design calculation suitable for rectangular wing. The reason for selecting rectangular plan-form is to ease the manufacturing and fabrication process of the wing. The design process began with defining the wing's dimensions, including span, chord length, and aspect ratio. Overall, the selection of a rectangular wing should provide a robust and efficient framework for achieving the project's structural objectives and ease in manufacturability.

3.2. Airfoil Selection

For the fixed wing UAV, the Clark Y is selected as the reference airfoil having a flat pressure surface which allows efficient lift to drag on lightweight model, providing good flight performance. The flat lower surface makes wing construction easier, as the wing ribs can be pinned directly onto the flat building board.

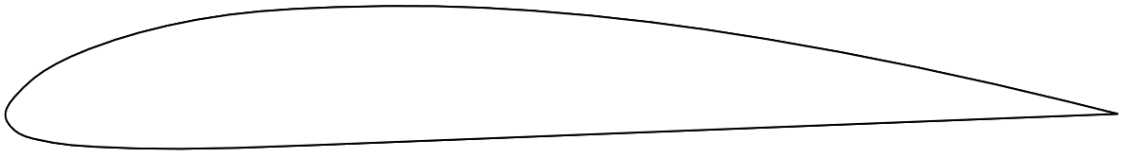

Figure 3.2: Clark Y Airfoil
[26]

1. Flight Requirements: Cruise/surveillance UAV.

2. Wing Dimensions and Characteristics:

   i. Span and Chord: The wing has a half span of 60cm and a root chord dimension of 25cm

   ii. Airfoil Thickness: Maximum airfoil thickness is 3cm at the root section.

3. Structural Components and Design:

   i. Primary Structure: The FE idealization of the wing primary structure includes ribs, upper and lower carbon fiber reinforced composite skins, and two cylindrical carbon fiber spars rod (8.5mm).

ii. Position of front spar: 18-25 percent of the chord length. The distance between the front spar and aerodynamic centre should be minimized to prevent torsion. Similarly, it should not be kept too close to the rear spar, as it would render the function of the front spar as futile.

iii. Position of rear spar: 62-65 percent of the chord length. The rear spar not only adds to the strength but also acts as a supporting member for the aileron (control surface used for the roll of aircraft).

iv. Distance between adjacent ribs: 6-8 cm. A higher distance would not only decrease the strength of the wing but also would destroy the aerodynamic shape required for the wing. At the same time, a lower distance would increase the number of ribs, adding to unnecessary weight to the structure. Further, a constant distance between the ribs allows easy calculation and fabrication[27].

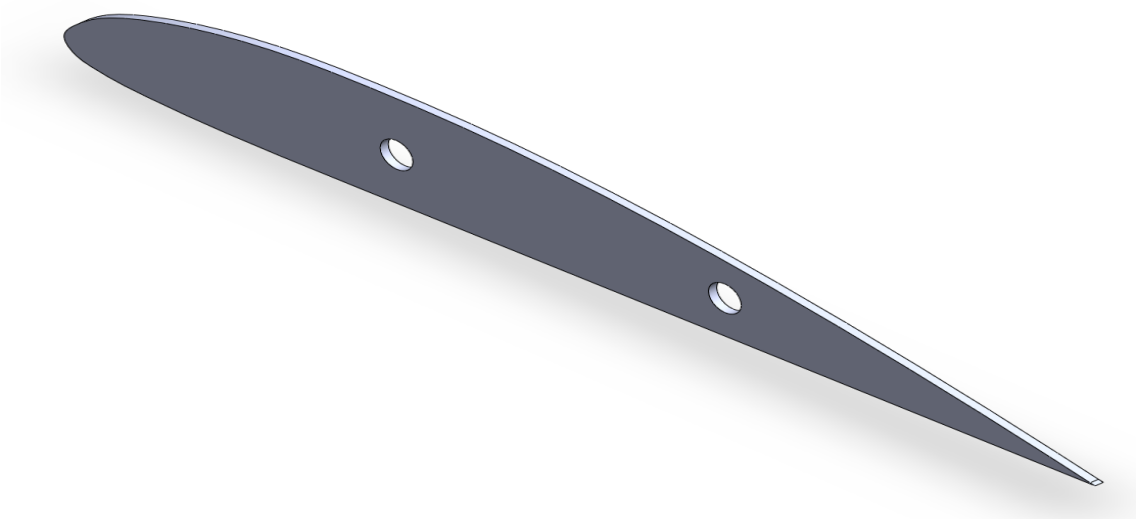

Figure 3.3: Rib Design

4. Aerodynamic Consideration:

i. Wing Shape Selection: The airfoil shape of the wing affects its lift and drag characteristics. So ClarkY airfoil which is suitable for sustained cruising with high value of lift-to-drag was chosen for this study[28]. A rectangular wing shape was chosen due to its suitability for non-high-altitude missions and ease of fabrication.

ii. Aerodynamic Center: The aerodynamic center of an airfoil is a crucial concept in aerodynamics. It is typically located approximately at the quarter chord point, where the moment coefficient remains constant regardless of the angle of attack. This point is significant because it allows to predict the aerodynamic behavior of an airfoil more accurately.

iii. Angle of Attack (α): The angle of attack, chosen at 5 degrees for this study, is a crucial parameter in aerodynamics. This value was chosen with an intent to study the wing behavior during cruising speed. This angle produces the most efficient lift-to-drag ratio for the airfoil, enabling the UAV to fly for longer distances.

iv. Wing Loading(n): The wing loading, or the mass of the UAV divided by the wing area, determines the size and shape of the wing. Higher wing loading requires a larger wing area to generate sufficient lift, while lower wing loading can allow for a smaller wing.

$$\begin{aligned}\text{Wing Loading}(n) &= \frac{\text{Mass of UAV}}{\text{Area of wing}} \\ &= \frac{M}{c \times s} \\ &= \frac{2}{(25 \times 120) \times 10^{-4}} \\ &= \frac{2}{0.3} \\ &= 6.67\,\text{kg/m}^2\end{aligned}$$

v. Aspect Ratio (A.R.): The aspect ratio of the wing, calculated by dividing the wing span by the wing chord, affects the lift-to-drag ratio. Higher aspect ratios result in longer and narrower wings, which are more efficient for high-speed flights. However, larger spans can make maneuverability more challenging. For cruise flight requirements, a medium wing span is proposed.

$$\begin{aligned}\text{Aspect Ratio}(A.R.) &= \frac{\text{span}^2}{\text{area}} \\ &= \frac{120^2}{3000} \\ &= \frac{14400}{3000} \\ &= 5.8.\end{aligned}$$

vi. Lift Force using Clavg

$$\text{Lift force using } C_{L_{avg}} = \frac{\text{Lift force}}{\text{Area} \times \text{Dynamic pressure}}$$

Given:

$$C_{L_{avg}} = 0.74 = \frac{\text{Lift force}}{0.15 \times 1.225 \times 0.5 \times 15^2}$$

Therefore:

$$\text{Lift force} = 15.29\,\text{N} = 1.558\,\text{kg}$$

$C_{L_{\text{avg}}}$ was calculated in XFLR5 in 3 different sections of 200mm each with values of 0.79, 0.75 and 0.68 for each sections. These are the requirements to be considered while modelling wing. The chosen measurements strike a balance between load-bearing strength and weight considerations. The table below provides key details about the Clark Y airfoil profiled wing, including geometric dimensions, aerodynamic performance metrics, and corresponding force values. This comprehensive dataset is crucial for analyzing the airfoil's aeroelastic behavior and serves as the foundation for an informed design approach[29].

3.3. Wing design and geometry consideration

The wing serves as a vital component of an aircraft, acting as a lifting surface when in motion through a fluid medium, typically air. The wing selected for the design calculations and the fabrication is the rectangular wing. The rectangular wing is specially selected since the mission requirement is not for high altitude flying and the rectangular section wing will be easy to fabricate. Rectangular wings better tolerate minor lapses in quality control/airfoil smoothness. The rectangular wings are the root chord stallers. If a situation occurs where stalling takes place, then the root chord will first stall followed by effects on the control surfaces like ailerons and flaps. This root chord stall will help the aircraft to regain stability again. The value of lift force generated by a wing is calculated using the lift equation:

$$L = \frac{1}{2} * C_l * \rho * A * v^2$$

Where,

L is the lift force

ρ is the air density

v is the velocity of the air relative to the object

A is the reference area (typically the wing area for an aircraft)

Cl is the coefficient of lift, which depends on the shape of the object and its AOA.

Cl value averaged for 5 degree AOA was found to be 0.79 for section of 0-200mm, 0.75 for section 200-400 mm and 0.68 for 400-600 mm.

Lift force for the sections for three sections simultaneously was 7.19, 5.56 and 2.48 N respectively.

3.4. Wing Characteristics

S.N.	Characteristics	Values
1.	Airfoil Name	Clark Y
2.	Root Chord	25cm
3.	Tip Chord	25cm
4.	Half Span	60cm
5.	Max Lift to Drag Ratio	15.281 at 5° AOA
6.	Aspect Ratio	5.8
7.	Taper Ratio	1
8.	Clmax	1.835
9.	Avg Cl	0.74
10.	Avg Cd	0.036
11.	Lift force (half span)	15.281
11.	Drag force (half span)	0.48

Table 3.1: Wing Characteristics at and 5° AOA

3.5. CAD Modelling

The wing model was developed using SOLIDWORKS, a versatile design software known for its seamless integration with digital fabrication systems and numerical analysis tools. This

approach ensures that the models are precise, adaptable, and efficient, enabling a smooth progression through manufacturing and analytical phases.

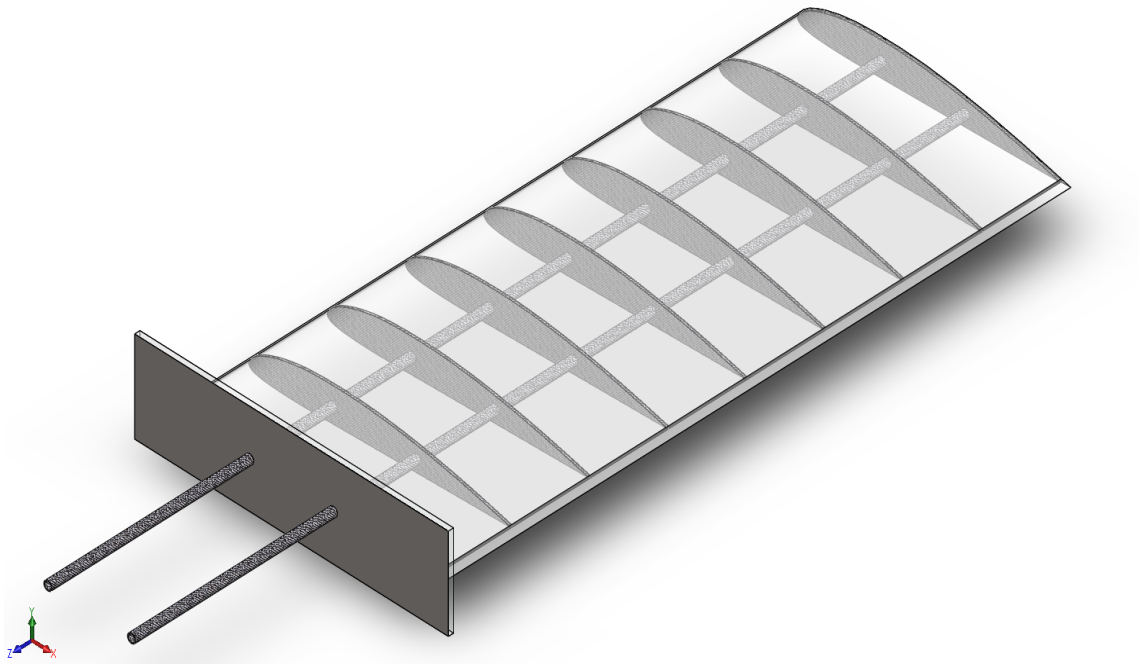

Figure 3.4: Detailed CAD model of the wing with 8.5mm carbon fiber rod and 2mm carbon fiber ribs frame structure, (3D rendered view)

The initial design of the semi-wing is shown in fig:3.4 which incorporate two cylindrical spars (8.5mm) and 9 ribs (2mm) positioned along half-span at equal distance (7.5mm). The spars were positioned at 25 percent and 55 Percent of the chord length, strategically located near the aerodynamic center. The spars served two purposes: structural reinforcement and attachment points for the carbon fiber reinforce composite skin [27].

3.6. Molding

For mold making there were few methods that were considered. The methods used were:

3.6.1. Silicon Molding

Silicone rubber molding is a method for shaping, forming, and fabricating silicone rubber parts and products using a heated mold. The process involves compressing or injecting silicone rubber into a mold where it takes the shape and form of the mold cavity. The processes used to produce silicone rubber molded parts are injection, compression, and transfer molding each of which relies on a mold made of steel or cast iron. A common use for silicone

molding is the creation of prototypes in order to examine a product design. Since the creation of metal molds is time consuming, labor intensive, and costly, silicone molds provide a cost-effective alternative. Aside from their use in prototyping, they assist in the creation of beta units for market testing and consumer input. Although 3D printing is ideal for quickly creating one off samples, silicone molds are capable of short production runs for testing.

For silicon mold solid surface is required beforehand. Small toy was used as solid to make silicon mold.

Steps for making silicon mold are:

- Silicon was poured into a mixing bowl.
- Hardener and accelerator were added, then mixed.
- The mixture was poured over the solid shape and left to harden.
- Caution should be taken in this step because the temperature rises very fast after adding the accelerator.
- This process was conducted at a temperature of 25 °C, and the setting time was around 20 minutes.

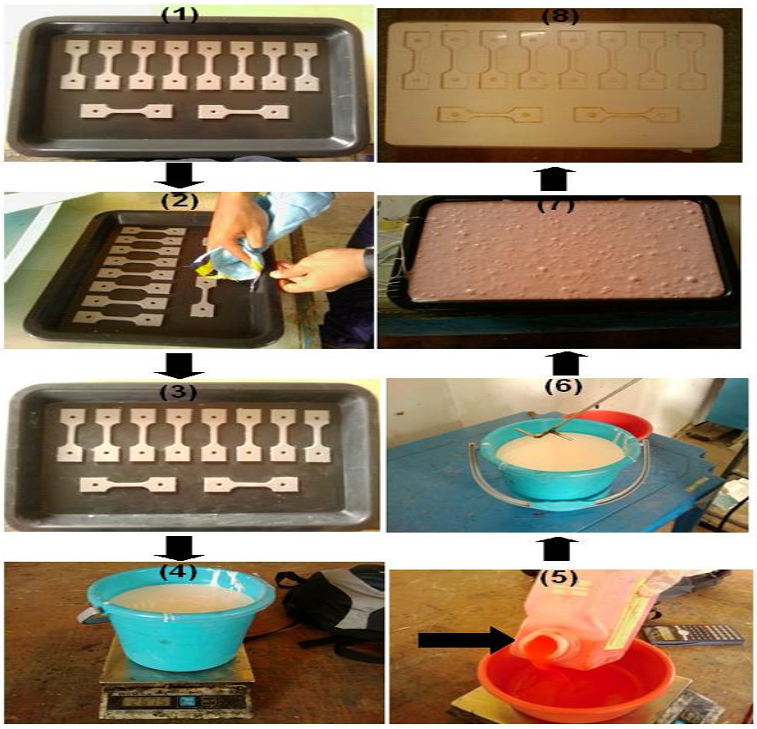

Figure 3.5: Silicon Molding Process

Figure 3.6: Mold generated from actual part

3.6.2. Foam

Styrofoam was used as the first choice for making the mold. As it is light weight, the sandwich model of fiber and foam could also be used for making the required design. Putty was used on the outer layer for two reasons:

- To create a layer between foam and sealer. Sealant is required so that the resin + hardener mix does not mix with putty.
- To give smooth finish for the foam surface.

Figure 3.7: Foam Molding

Steps:

- A shape design was made in any CAD software. Here, we have used SOLIDWORKS for the shape design.
- The design was cut on a 3-axis CNC foam cutter.
- Putty was applied to the outer layer and allowed to dry.
- Sandpaper was applied where required after drying.
- Sealer was applied to check for any pores where it might penetrate the putty layer.
- The fibre and resin + hardener + accelerator mix was applied for the required number of layers.

3.6.3. 3D Printing

For the fuselage making 3D printed design was taken. PLA filament was used for making the shape. As the shape was sturdy there were no complexities like in foam.

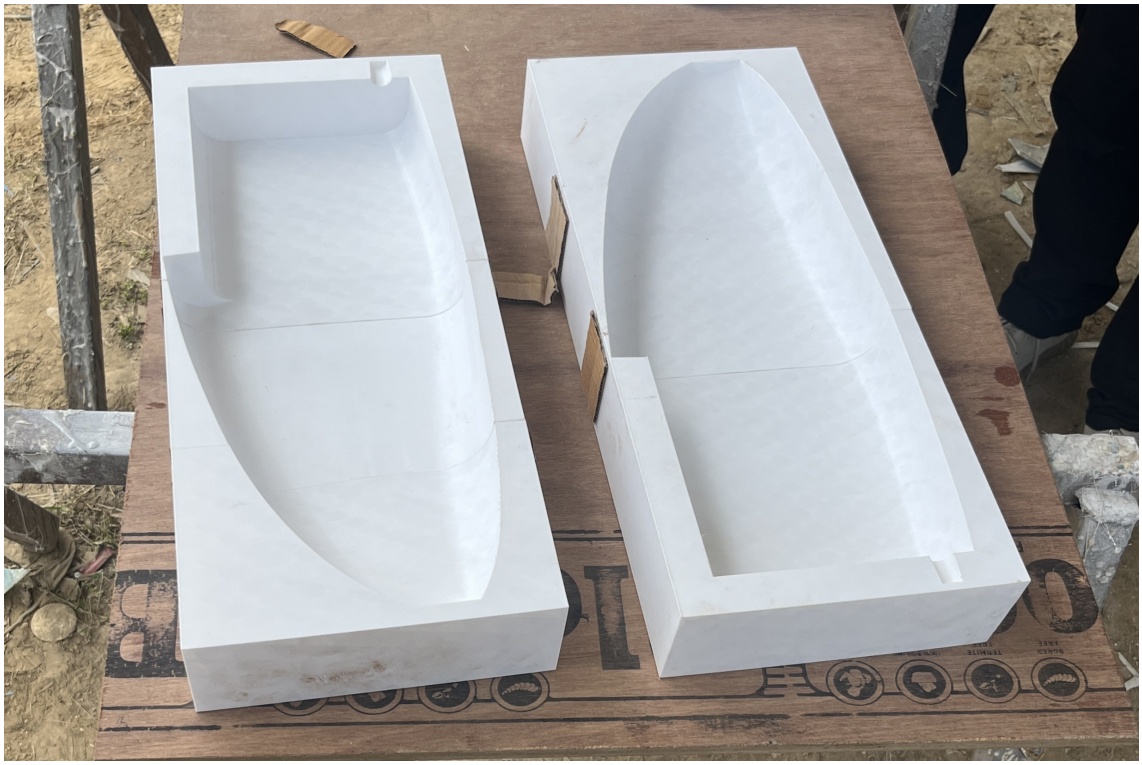

Figure 3.8: 3D Printed Part

Steps:

- Make a design of the shape in any CAD software. Here, we have used SOLIDWORKS for the shape design.
- Releasing wax was applied over the inner surface where the mix was applied.
- Sealer was applied to check for any pores where it might penetrate the putty layer.
- The fibre and resin + hardener + accelerator mix was applied for the required number of layers.
- Wait for the mix to dry and solidify. For a temperature of 28 °C, 10 minutes was sufficient.

3.6.4. Wood

MDF wood was used as the type for making mold. Female fibre mold was obtained from this. Simply it could be used as male mold too. Steps for making fibre mold from wood is:

- 3D design was made in SOLIDWORKS.

- CNC cutter was used to cut the wood.
- Primer was applied to the surface to make the surface smooth.
- Upper and lower surface were separated using cardboard and paper tape.
- Resin + hardener mix was then applied to upper and lower surface separately and left to dry.

Figure 3.9: Wood Part

3.6.4.1 One Part Molding The one part open face mold is the simplest form of silicone rubber mold. It is ideal for flat back masters without undercuts and is good for molding rigid materials like ceramics and silicone rubber.

- Step One - The master, which is the part design, can be created using 3D printing and made of a plastic resin. Its surface should be free of detail marks and washed to remove any tackiness.
- Step Two - The master must have a flat back with a small draft angle, which is a slight taper along the edge of the master. Limited tapering makes it possible to easily separate the master from the mold. The mold housing should be made of non-porous material with a flat bottom.

- Step Three - Mold release is applied to the mold housing and master. Once applied, it takes ten minutes for it to dry.
- Step Four - The silicone rubber solution should be carefully mixed and be vibrated to remove any air bubbles. The mixture is then poured into the mold housing starting with the lowest part of the housing and gradually moving upward.
- Step Five - The curing process takes one hour to one week depending on the type of silicone rubber. Once the mold is completely cured, silicone is removed from the containment box, and the master is removed from the silicone mold. The completed mold can be used multiple times by spraying the silicone mold with the release solution.

3.6.4.2 Two Part Molding The beginning steps for the creation of a two part silicone mold are the same as those for a one part silicone mold, which is the creation and selection of the master.

Figure 3.10: Two Part Molding

- Step One - In the first step, the master is embedded in clay, which should be sulfur free and oil based. This part of the process defines the parting line. The master is positioned in a mold box where a pour hole and air hole are added.
- Step Two - For proper alignment of the two halves of the mold, keys that have a tongue and groove appearance are evenly placed in the clay around the mold. Mold keys are holes in the clay that will be filled with silicone rubber and serve as guidance during the casting process.

- Step Three - A specific amount of silicone rubber is mixed to completely cover the first half of the mold. This aspect of the process is carefully calculated for determining the amount for the second half of the mold. The mixture is poured over half of the master and is allowed to cure.
- Step Four - The sides of the mold box are removed to expose the clay, master, and cured silicone. The master is left in the silicone, and the clay is removed along with the silicone in the mold keys.
- Step Five - The mold box is constructed around the master and silicone. A release agent is applied to the master, mold keys, and silicone prior to pouring the silicone rubber. As with the original pouring, the silicone rubber is carefully and precisely measured such that it easily flows over the master, mold keys, and silicone.
- Step Six - The finished two part silicone rubber mold is removed from the mold box and separated to remove the master. The halves of the mold form the cavity for shaping a part, component, or piece of art.

3.6.5. Resin-Hardener Mix

Resin is the material that bounds fibre and hardener is the chemical for curing resin coated upon the fiber. Consideration has to be done for this process in following way:

- Exact quantity of resin was poured in the mixing bowl.

  (For resin with high viscocity force might have to be used for pushing it out of the stored bottle. Also, for resins with low viscocity, carefulness should be given not to overflow resin.)

- Hardener was poured into the mixing bowl in exact quantity.

  (Special consideration was given for pouring of hardener. If the weight of hardener is more than required while pouring then the ratio won't be standard. Or otherwise quantity of resin must be added more than estimated early.)

Figure 3.11: Resin Hardener mixing up

3.6.6. Hand Layup Process

For the hand layup of fiber cloth, resin has to be applied in certain direction only. For single layer, brush was moved in vertical direction only for skin.

For double layering, two directions perpendicular to each other were marked and resin were applied. Consideration should be made for any air trapped inside fiber layer. If any air is trapped inside then roller should be rolled from top side toward open edge.

After resin is applied make sure so that the setup doesn't move. If the setup moves then layup process must be repeated.

3.7. Curing

During actual composites processing, the resins do not begin to cure prior to direct exposure to UV light. While the irradiating light source will normally be tailored to the requirements of the specific material and process design even achieved curing of glass fiber/epoxy laminates on exposure to sunlight. This "cure on demand" has implications for handling the material in industrial production. Light curing resins can be pre-mixed and stored at room temperature as one part systems with no mixing required prior to processing. The shelf life is long when compared with heat curing pre-mixed systems. The characteristics of the resin systems allow complete impregnation of the fiber material without premature gelation. The

resin is then cured in a second step. This separation of impregnation and curing phase facilitates prediction of resin flow for resin injection/infusion type processes, since the viscosity of the liquid resin does not change during impregnation of the reinforcement textile .[19]

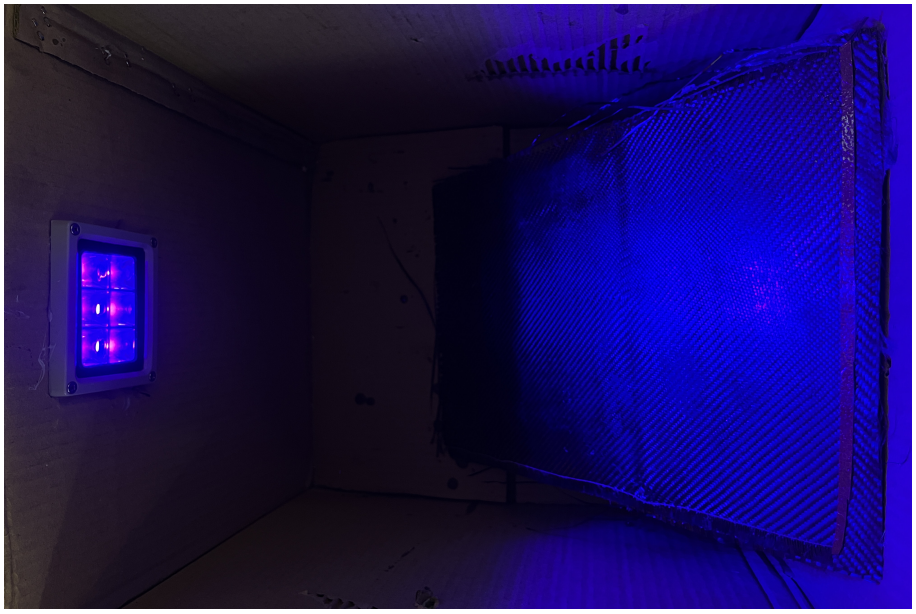

Figure 3.12: UV Curing

3.8. Glass Fiber Making

There were 2 molds made as female and male mold. For glass fiber, female mold was used. As female mold has two separate parts there were two parts made up of glass fiber too. The ratio of fiber to resin is used as discussed in the introduction section though there is no hard and fast rule for usage for quantity.

Figure 3.13: Glass Fiber Wing

Steps for glass fiber making:

- The ends of fiber was marked by exactly placing on the mold.
- Fiber was then cut. (Remember to cut the fiber cloth by sharp objects. If blunt object is used, then there is chance of fiber entanglement.)
- The releasing wax was applied on mold. (This step is crucial otherwise the surface of fiber will stick to mold.)

On the basis of required weight and strength resin and hardener were mixed. 100 gm of epoxy laminating resin and 40 gm of hardener were used as per the standard ratio of 100:40 for resin to hardener.

- Fiber cloth was laid upon the mold with tightening of ends.
- Resin was then applied in directions mentioned below in hand layup process.
- Curing was done in natural light and product was taken out.

3.9. Carbon Fiber making

Male mold was used for making wing from carbon fiber. Wood mold was used and a single part skin was made. Steps for making the skin were similar to glass fiber which are discussed below:

- The ends of fiber was marked by exactly placing on the mold.
- Fiber was then cut. (Remember to cut the fiber cloth by sharp objects. If blunt object is used, then there is chance of fiber entanglement.)
- The releasing wax was applied on mold. (This step is crucial; otherwise the surface of fiber will stick to mold.)

On the basis of required weight and strength resin and hardener were mixed. 100 gm of epoxy laminating resin and 40 gm of hardener were used as per the standard ratio of 100:40 for resin to hardener.

- Fibre cloth was laid upon the mold with tightening of ends.
- Resin was then applied in directions mentioned below in hand layup process.
- Curing was done in natural light and product was taken out.

3.10. Test Specimen

We designed our test specimen following the ASTM D3039 standard, a widely used method for determining the tensile properties of composite materials. While there are various types of composites, ASTM D3039 specifically applies to those with a polymer matrix reinforced by high-modulus fibers. Our test specimen features a minimum thickness of 3 mm, including the gripping surface, where rubber pads are used to securely hold the specimen during tensile testing in a Universal Testing Machine (UTM).

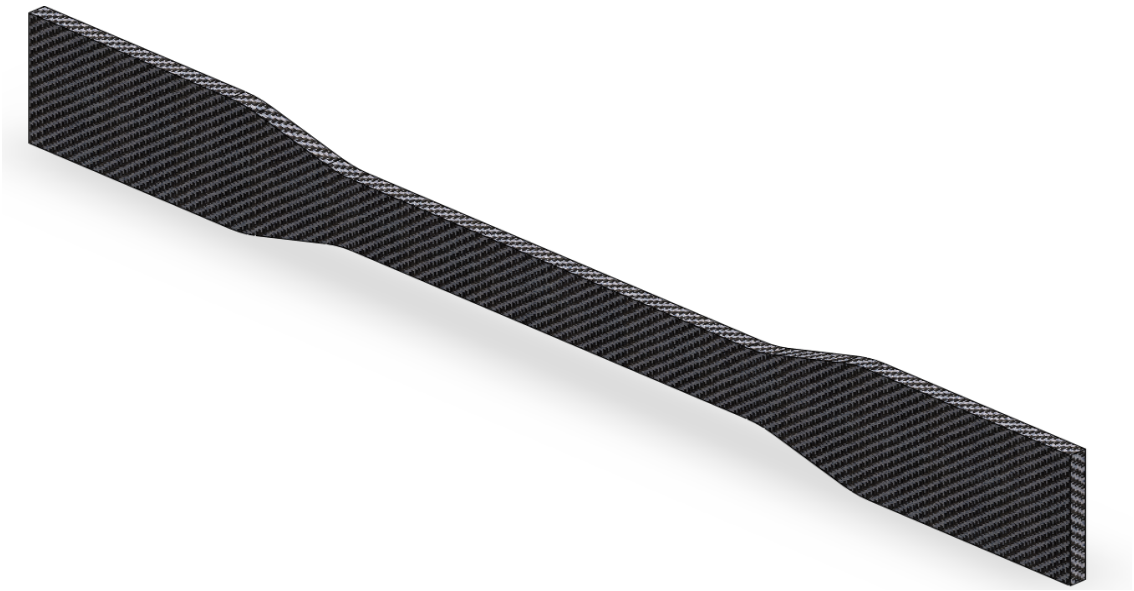

Figure 3.14: CAD Design of Test Specimen

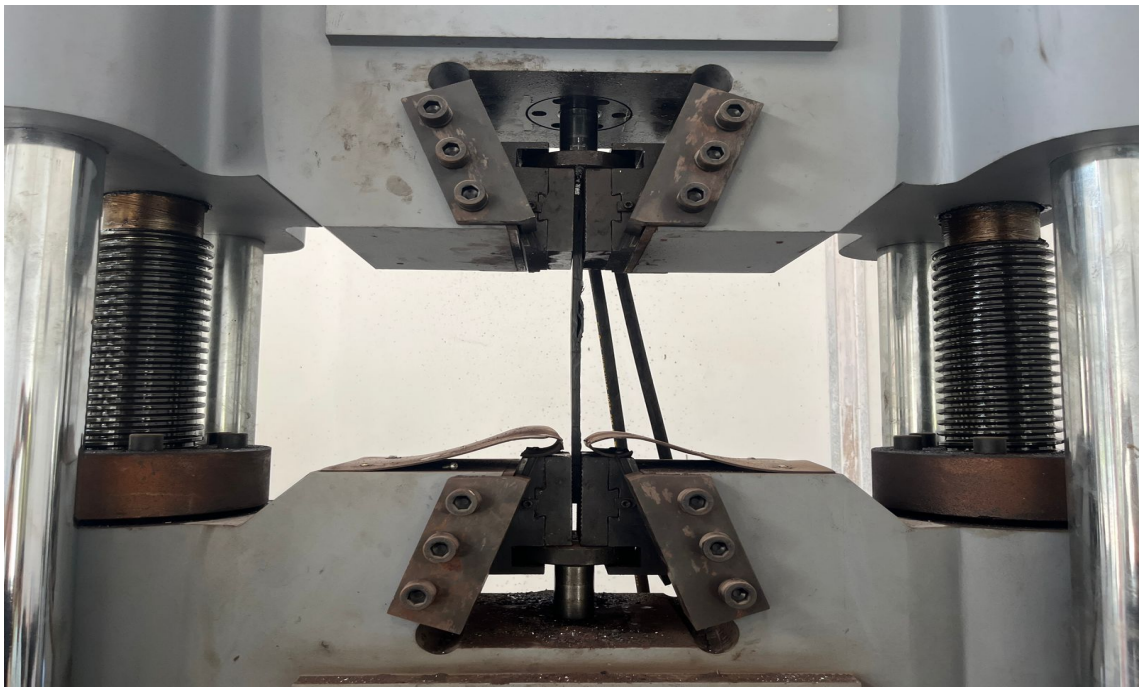

Figure 3.15: UTM testing Setup of Test Specimen

3.11. Finite Element Analysis

We used Finite Element Analysis (FEA) to estimate the structural properties of the wing in advance of using experimental testing. This computational technique was pivotal to the design process, allowing simulations of how the wing structure would respond under defined

boundary conditions. It also enabled predicting potential localizations of stress or failure that could be validated experimentally. A model of the composite wing structure was designed in SOLIDWORKS software to obtain the actual properties of its physical properties such as real dimensions and geometry. Then the detailed model of the carbon fiber wing assembly and wall clamp setup was imported into ANSYS. Changes were made in Space Claim environment in order to ensure the geometry is appropriate for the following analyses. Refining intersected regions, removing redundancies, and finalizing a clean and error-free geometry were among those adjustments. Material properties were carefully assigned to each component of the assembly. The spar rod, skin and ribs was defined as carbon fiber woven material and the clamp was defined as acrylic glass. For materials not available in the ANSYS material library, custom material definitions were created, ensuring their mechanical properties accurately reflected real-world data. Before advancing to analysis, the assembly's integrity was thoroughly verified. Connections between components were inspected to ensure there were no gaps or overlaps that could affect the accuracy of load transfer. This verification step was critical for ensuring reliable and precise simulation results.

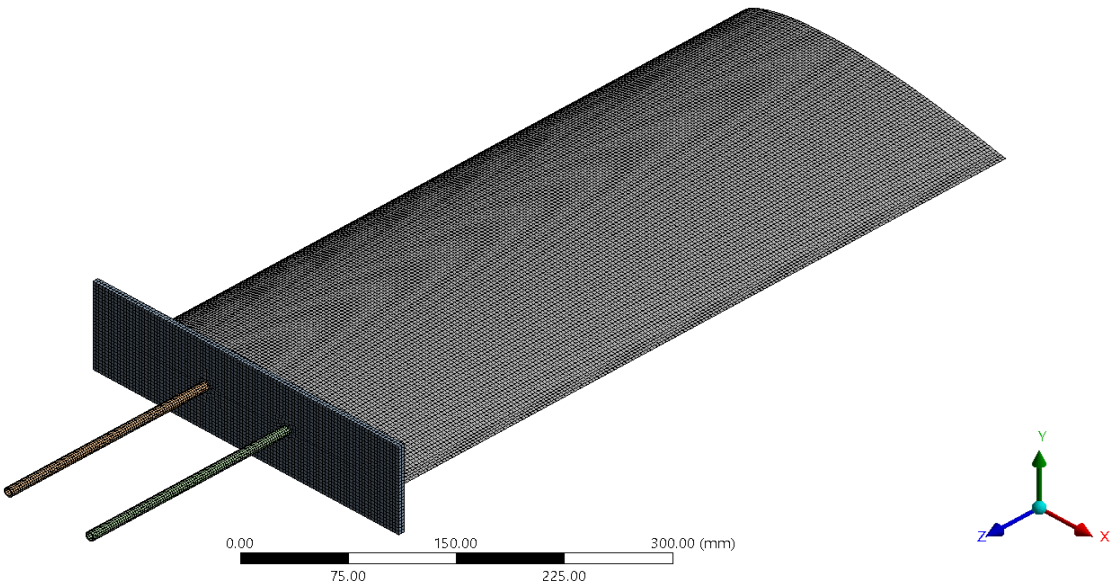

Figure 3.16: Meshing of wing

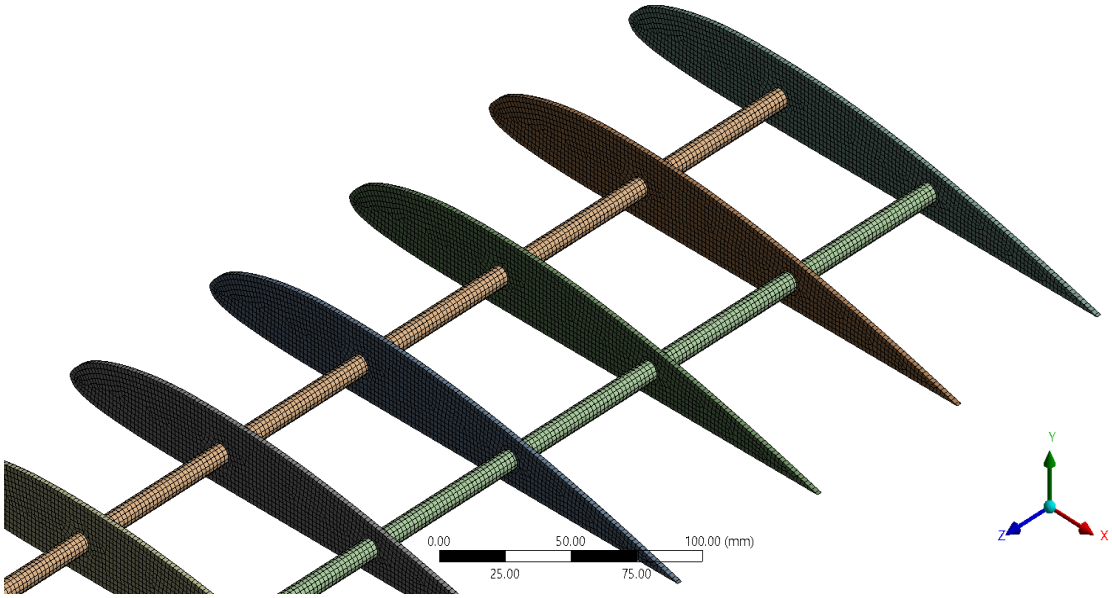

Figure 3.17: Meshing of internal structure of wing

Due to the diverse characteristics of the components, a quadrilateral dominant meshing strategy was employed in a critical components with complex geometries, such as the spar rods and ribs, for structured finer mesh to capture intricate details. The carbon fiber skin was meshed with a maximum element size of 3mm, while the internal structures utilized a finer minimum mesh size of 2mm. Through several preliminary meshing iterations, an optimal mesh density was established to balance geometric accuracy and computational efficiency. This approach ensured that the intricate features of the assembly were well-represented without overloading computational resources. A detailed, zoomed-out view of the differentiated mesh is provided in Figure 3.17. The meshing approach resulted in a total of 64,187 mesh elements and 4,38,818 nodes. In ANSYS, nodes serve as calculation points for physical properties, while mesh elements connect these nodes, dividing the structure into smaller, manageable parts. The mesh elements define the structural shape and behavior, while the nodes allow the computation of parameters such as stress, strain, and deformation at specific locations.

3.12. Structural Analysis under Limit Load

After completing the preparatory steps, the loading and boundary conditions were defined as shown in Figure 3.18. The limit loads previously calculated for different span sections were applied to the corresponding faces, simulating the aerodynamic pressures experienced in flight.

To replicate the experimental setup:

Clamping plate: Displacement in the z-direction was fixed, while x and y directions remained free.

Cylindrical spars: Displacement in x and y was restricted, allowing movement in the z-direction.

The analysis settings were then configured, including selecting the solver type, allocating processing cores, and defining output parameters. Finally, the simulation was executed.

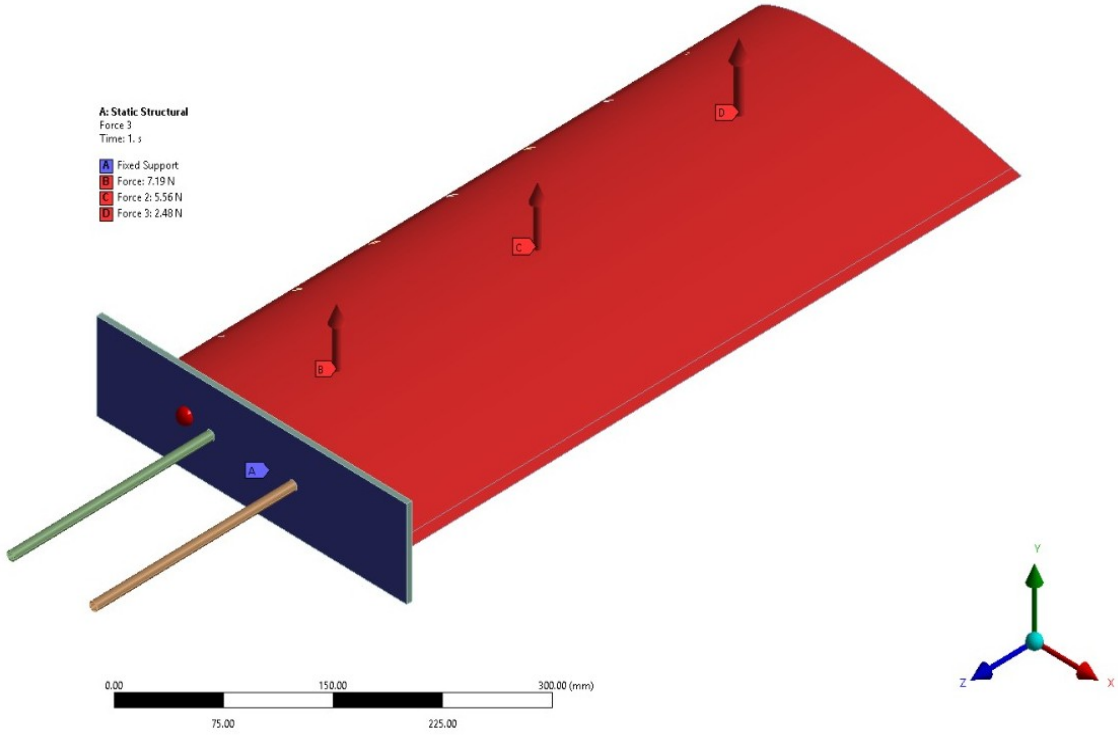

Figure 3.18: Setup of boundary and loading conditions for static structural testing.

3.13. Fabrication of wing.

Following the fabrication of the carbon fiber wing skin and internal components, the assembly process was carried out to ensure proper structural integration and aerodynamic efficiency. The assembly involved precise alignment and bonding of the spars, ribs, and wing skin to achieve a robust and lightweight design.

1. Composite Material Composition

The composite material consisted of carbon fiber cloth (240 GSM, twill weave) impregnated

with a thermosetting epoxy resin matrix, with a resin-to-hardener mixing ratio of 100:40 by weight, ensuring proper curing, fiber wet-out, and minimal void content. The layup configuration included [0°/90°] orientation for primary load-bearing capacity, [±45°] for shear resistance and torsional stiffness, and woven twill fabric for uniform mechanical properties. The internal frame, including spars and ribs, was reinforced with unidirectional carbon fiber strips for localized strengthening at high-stress regions, This strategic fiber orientation and fabrication method resulted in enhanced load distribution, superior resistance to bending and torsional deformation, and a lightweight yet robust construction, optimizing payload efficiency and flight endurance for UAV applications. The integration of advanced composite layup techniques ensured high structural efficiency, making the fabricated wing well-suited for applications requiring durability, aerodynamic performance, and weight optimization.

The bond between fibers and the matrix material is paramount to prevent fiber-related anomalies, as it ensures effective load transfer, enhances mechanical strength, and minimizes delamination risks. Proper selection of the resin system, surface treatment of fibers, and optimized curing processes are critical factors in achieving a reliable fiber-matrix adhesion, ultimately improving the composite's durability and performance in aerospace applications.

2. Development of Mold

To fabricate the wing skin, a wooden male mold was developed using a Woodworking 3D 1530 CNC Machine. The use of digital manufacturing tools played a crucial role in ensuring precision, accuracy, and repeatability in the mold development process. CNC machining provided high-resolution contouring of the wing profile, ensuring the aerodynamic shape was maintained with minimal surface irregularities. The male mold configuration was chosen to facilitate proper fiber layup and resin distribution, ensuring a high-quality composite surface finish.

The integration of CNC machining streamlined the fabrication process, allowing for rapid iterations and modifications to the mold design. Unlike foam molds, which require careful sanding and a demolding layer, the wooden mold provided a durable and stable platform for composite layup, minimizing deformation during the curing process. Fine surface finishing was achieved through post-machining sanding to eliminate roughness, ensuring uniform fiber adhesion during the layup.

By leveraging digital manufacturing techniques, the mold development process achieved high accuracy, repeatability, and efficiency, reducing manual errors and ensuring consistency in composite fabrication. This approach significantly enhanced the overall structural integrity and aerodynamic performance of the final wing prototype.

3. Layup and Curing Process of wing prototype

The layup and curing process played a vital role in ensuring the structural integrity and surface quality of the carbon fiber wing prototype. Prior to the layup, the wood mold was coated with a layer of releasing wax to prevent adhesion between the composite skin and the mold surface, facilitating seamless demolding. The resin-hardener mixture, prepared in a 100:40 weight ratio, was applied uniformly over the mold surface to act as an adhesive layer. The pre-cut carbon fiber cloth was carefully laid over the mold, with the tip section secured using clips to maintain the fiber orientation and prevent displacement. A second layer of the resin-hardener mixture was applied with a fine-grade brush to ensure full impregnation of the fabric, eliminating voids and promoting optimal bonding between the fibers and matrix.

The wing skin was then left to cure under direct sunlight at an ambient temperature of approximately 21°C, with a settling time of 15 hours, allowing the matrix to fully harden while preserving the aerodynamic profile. For the rib sections, the same layup procedure was followed, but curing was performed using a UV lamp, where the temperature was maintained at approximately 10 hours to expedite the curing process and ensure uniform resin hardening.

Resin to Fiber Ratio

CF Fabric Density = 240 gsm

- Fiber : Resin = 40:60

The fiber used to make the specimen was:

$$41 \times 4.5 \times 6 = 1107 \text{ cm}^2 \Rightarrow \text{Total area of fabrication} \tag{3.1}$$

Fiber Mass:

$$0.1107 \times 240 = 26.56 \text{ g} \tag{3.2}$$

Required Resin:

$$\frac{26.568 \times 0.6}{0.4} = 39.85 \text{ g} \tag{3.3}$$

The strategic use of resin and fiber layers was derived from literature reviews to optimize the wing's structural properties. The multi-step curing process ensured proper adhesion, reduced void content, and enhanced mechanical performance. This method not only streamlined

the manufacturing process but also maintained the dimensional accuracy of the prototype, making the final product lightweight, durable, and suitable for UAV applications.

4. Internal Frame and Skin Assembly

The internal frame of the wing was designed to provide structural support while maintaining a lightweight configuration. Two 8.5mm carbon fiber rods were used as the primary spars, selected for their high tensile strength and stiffness, ensuring the wing could withstand aerodynamic and structural loads effectively. The ribs were designed in SolidWorks and exported in DXF format, which was then processed in RDWorks V8 for CNC laser cutting. However, due to limitations in the CNC laser cutter, the machine could only etch the rib patterns rather than fully cutting through the material. Consequently, the final cuts were completed manually using a grinder to achieve the required precision.

To ensure proper fitment and accuracy, 3D rib templates were printed using a 3D printing machine, serving as guides for shaping the cured carbon fiber ribs. The cured carbon fiber sheet was then cut into the rib pattern using a grinder, ensuring a precise fit within the wing assembly. Once the spars and ribs were assembled, resin was applied over the structure to enhance adhesion and reinforce the frame.

For the final assembly, the internal frame was inserted into the fabricated carbon fiber skin, ensuring a seamless integration. The spars and ribs worked together to preserve the aerodynamic shape while effectively distributing structural loads. This combination of high-strength carbon fiber spars and precisely cut ribs resulted in a lightweight yet durable wing structure, optimized for UAV applications.

Figure 3.19: Process involved in fabricattion of carbon fiber wing

3.14. Microscopic Analysis

The methodology for microscopic assessment and image analysis involves four key stages: sample preparation, microscopic imaging, image processing, and experimental validation. This structured approach ensures precise characterization of fiber distribution, resin penetration, and alignment uniformity.

i. In the sample preparation phase, the specimen is carefully cut and polished to achieve a smooth surface, ensuring high-quality imaging. If required, chemical etching is applied using appropriate reagents to enhance the visibility of microstructural features such as grain boundaries, fiber distribution, or crack propagation.

ii. Following preparation, microscopic imaging is conducted using an scanning electron microscope (SEM), depending on the required resolution and analysis depth. The microscope's magnification, focus, and illumination are adjusted to optimize image clarity. High-resolution images are captured and stored in appropriate formats (e.g., TIFF, PNG) to preserve detail for further processing and quantitative evaluation.

iii. The image processing phase involves preprocessing, which includes grayscale conversion (if necessary), noise reduction using Gaussian or median filters, and contrast enhancement through histogram equalization.

iv. The final step, experimental validation and statistical analysis, ensures the reliability of extracted data. The measured parameters are compared against manufacturer specifications or experimental benchmarks.

In this study, the primary focus is on determining the microstructural diameter of fibers, resin-hardener distribution, and carbon fiber alignment, ensuring precise characterization of composite material properties characterization by integrating experimental imaging techniques.

Figure 3.20: Microstructural Assessment of test specimen

3.15. Data Collection Using High Speed Camera (Chronos 1.4)

To measure the vibration response, a strip of white tape was applied to the tip section of the carbon fiber wing as a visual marker for displacement tracking. The high-speed camera, set to capture at 1000 fps with a frame size of 1280x1024 for a 4-second duration, recorded the wing's movement. A rubber hammer was used to introduce vibration to the wing tip, ensuring minimal contact time. The setup featured a white background and optimal lighting conditions, providing high contrast to accurately track the wing's displacement. The camera was positioned at the ideal angle to clearly capture the movement of the wing tip.

The TIFF data was collected for two repeated measurements under varying load conditions: no load, and full load. The captured TIFF data were processed in MATLAB to generate displacement-time plots, which were then subjected to Fast Fourier Transform (FFT) analysis to determine the natural frequency of the wing's vibration.

Additionally, a wind tunnel test was conducted to simulate real aerodynamic loading conditions. The carbon fiber wing was positioned and the wind tunnel was operated at a maximum velocity of 8.2 m/s. Captured frames were then processed to determine vibrational frequency. The experimental setup for the wind tunnel test is shown in figure 3.21.

Understanding the modal frequencies and damping properties of the carbon fiber wing is crucial for preventing resonance, optimizing performance, and implementing effective vibration control measures. It also forms the basis for structural health monitoring, allowing for the early identification of any damage or deterioration. This comprehensive analysis ensures the safety and reliability of the carbon fiber wing, guaranteeing that it operates within the designed dynamic limits.

Figure 3.21: Vibration monitoring Setup

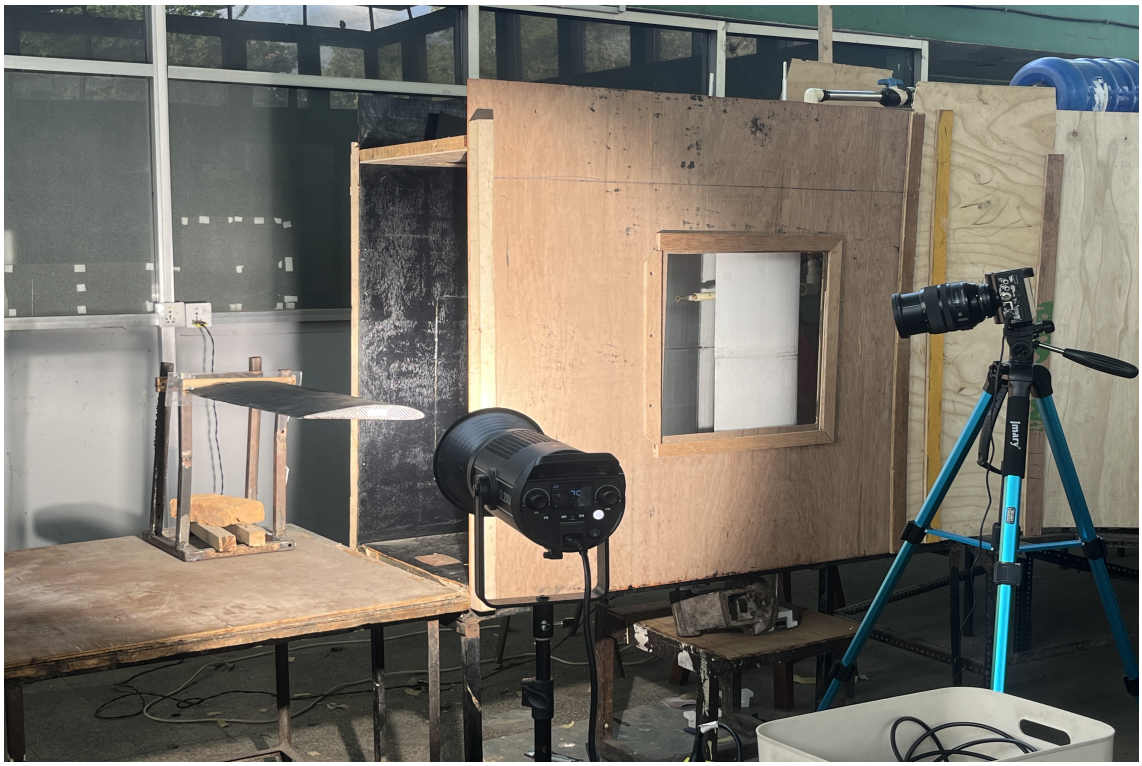

Figure 3.22: Wind Tunnel Testing setup of wing

4. RESULTS AND DISCUSSION

4.1. Mold

Four types of molding techniques were studied with physical usage procedure kept in check. Upon considering the obtained fabricated molds, following conclusions were made:

Material	Time	Complexity	Money
Silicon	3	3	4
Foam	4	4	1
3D Printing	2	2	4
Wood	1	1	2

Table 4.1: Comparison of different mold techniques

Points were given as 1 being the best choice for the category and 4 being the worst. From the result we can see that the mold of wood with primer is beneficial for usage. Though the choice depends upon the use case provided that the silicon or 3D printed mold might be useful for two part piece fabrication.

Two part molds of 250GSM glass fibre was obtained with smooth surface inside. The finishing of the inside surface was at par with the requirement.

Figure 4.1: Foam molding failure

In the making of mold from foam, failure occured due to sealer reaching foam through the

cracks in putty. Sealer oozes out the air trapped in foam and acts like vacuum. So the putty fails inwards to fill in the space.

Figure 4.2: Silicon Mold Failure

This failure is due to overweight of accelerator used. Temperature rose exponentially after use of accelerator and the time for setting was very less. Due to this, cracks started to form and the structure disintegrated.

Wood cut from cnc was then used for making the skin of carbon fibre of following shape.

Figure 4.3: Wood Wing Design

4.2. Fiber Fabrication

Glass fiber was made from two part mold and carbon fiber was made up of one part. Glass fiber wing with upper surface remove is shown below which has total weight of 300 gm. This is due to the reason that ribs were made up of double layering. Consideration for use of balsa wood ribs or single layer carbon ribs was made for carbon wing.

The weight was also partly due to the overestimation of resin required.

The weight of end product made up of carbon fiber had weight of 272 grams with density of 1789.95 $\mathrm{g\,m^{-3}}$.

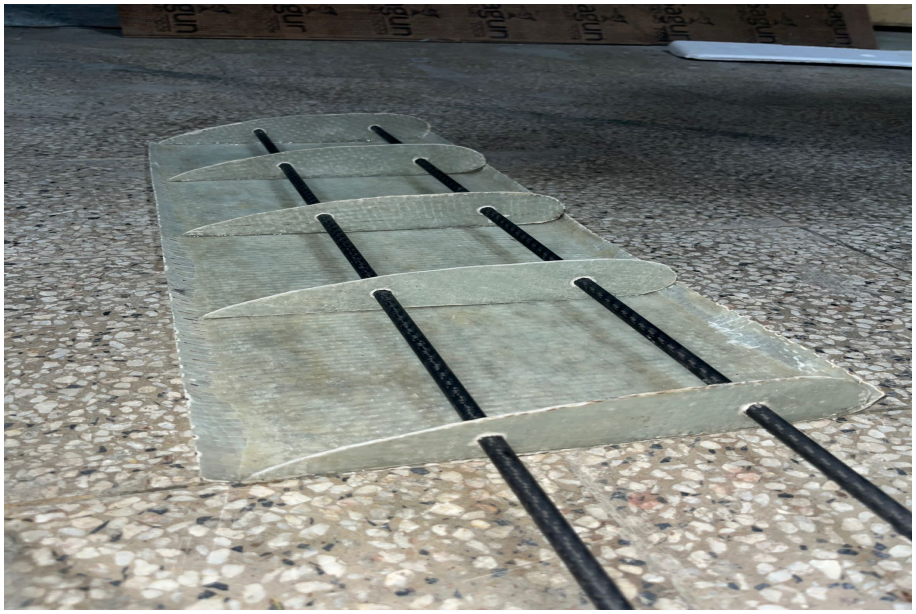

Figure 4.4: Glass Fiber Wing

Figure 4.5: Carbon Fiber Wing Skin

4.3. Curing

For the objective of finding curing time of epoxy resin for different temperatures following results were obtained.

For a temperature range of 25-28 °C curing time was found to be around 9 hours.

For a temperature range of 20-25 °C curing time was found to be around 15 hours.

For a temperature range of 4-12 °C curing time was found to be around 22 hours.

Also, UV curing was found to be good solution to this problem but due to the small size of the UV curing setup, whole wing couldn't be cured in it.

The wavelength of UV lamp used was 405 nm.

4.4. FEA Results

4.4.1. Static Structural Analysis of Wing

Following the analysis, key structural parameters such as total deformation, stress distribution, and strain were assessed. Our wing design, consisting of two cylindrical spars and nine ribs, showed localized stress concentrations at the connection points between the rear spar

and ribs. The total deformation was measured at 3.16 mm, demonstrating an improvement over the findings of Sandipan Roy [30] , where a deformation of 4.65 mm was reported. This reduction in deformation indicates a more structurally efficient design, reinforcing the effectiveness of the selected materials and configuration.

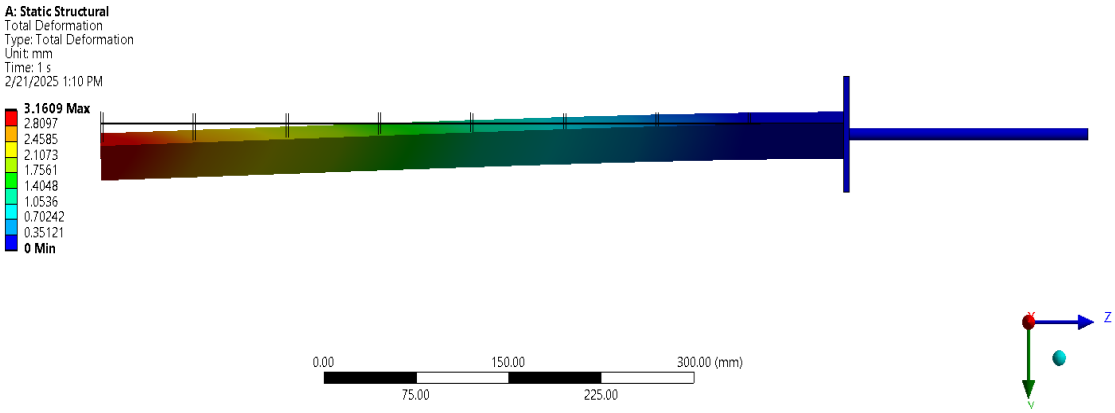

Figure 4.6: Deformation Contour of wing under limit load(3.16mm)

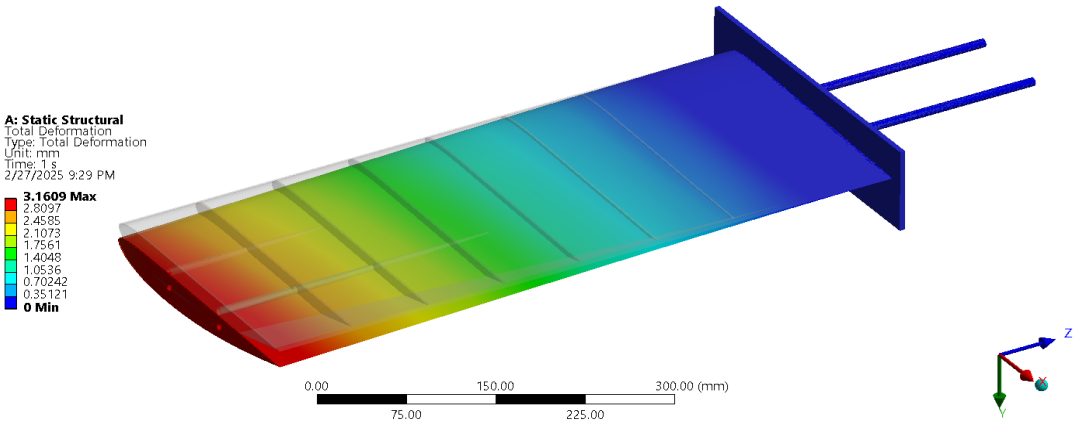

Figure 4.7: Total Deformation Contour of wing under limit load(3.16mm)

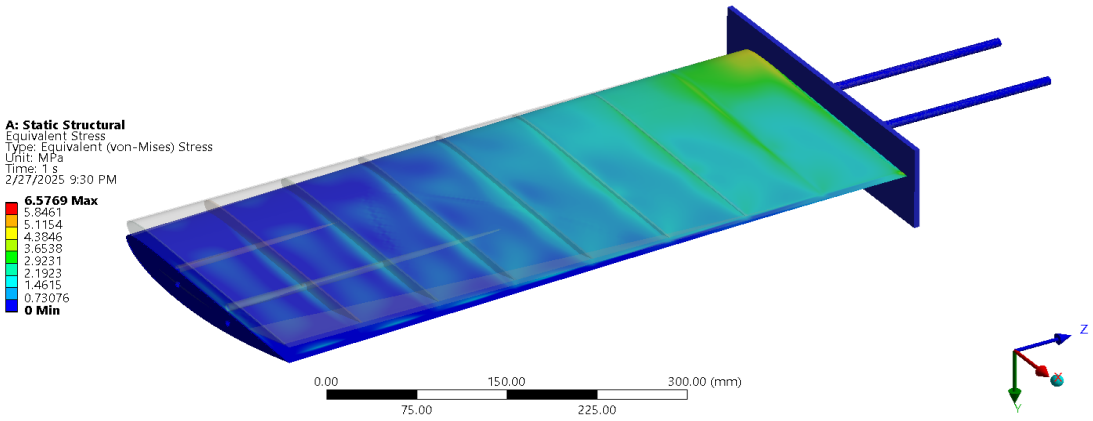

Figure 4.8: Equivalent Stress contour under limit load

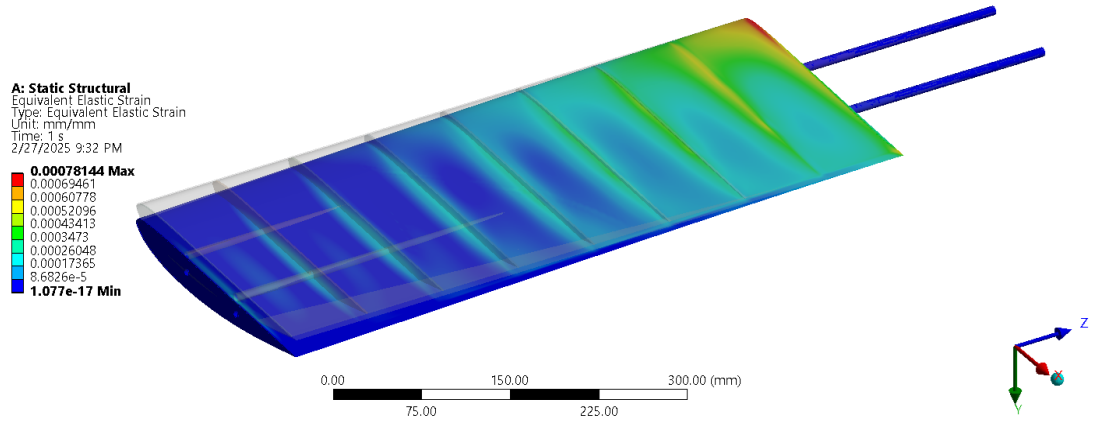

Figure 4.9: Contour plot highlighting regions of high equivalent elastic strain.

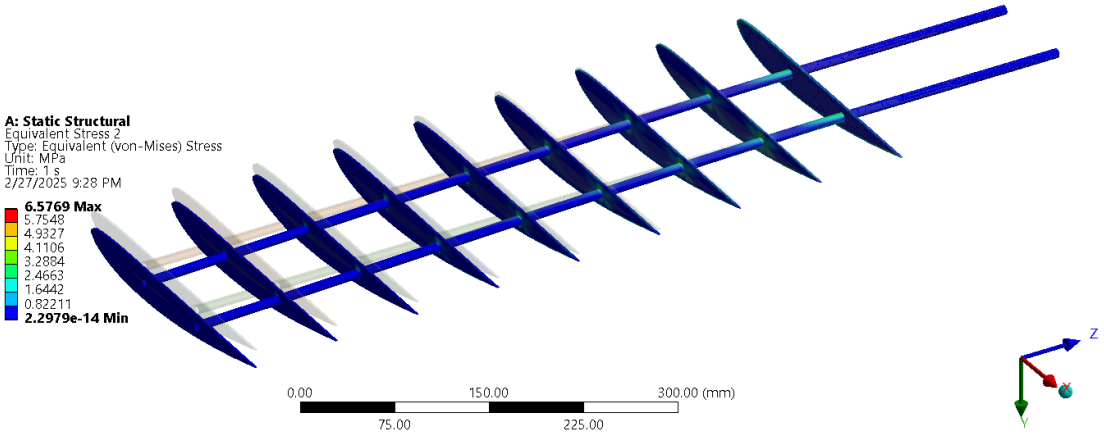

Figure 4.10: Contour plot highlighting stress concentration regions at internal structure.

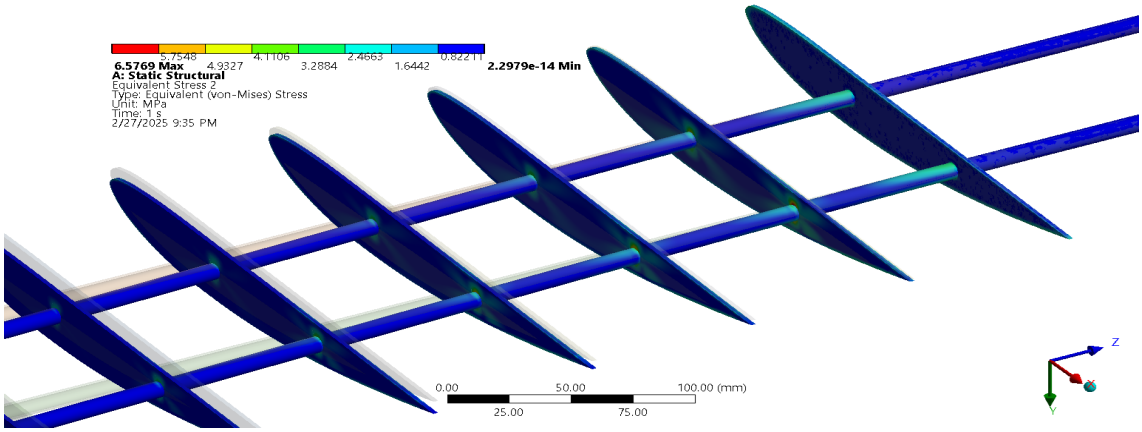

Figure 4.11: Contour plot highlighting stress concentration regions at internal structure.

Excessive wing flex or deformation can negatively impact stability and control, making precise maneuvering more difficult. The assessment of deformation and stress metrics was instrumental in refining the wing design, leading to modifications such as optimizing the spar arrangement and adjusting the thickness of critical structural elements. Specific changes were implemented to alleviate stress concentrations, particularly along the trailing edge, effectively reducing both stress and strain.

To enhance structural rigidity while maintaining an optimal strength-to-weight balance, the final design incorporated two cylindrical carbon fiber spars and nine ribs, each 2mm thick, constructed from carbon fiber infused with resin and hardener. This rib thickness was chosen to provide adequate structural integrity while minimizing weight, ultimately improving aerodynamic efficiency and overall performance.

4.4.2. Result from Modal Analysis

The vibrational characteristics of the wing structure were examined through numerical analysis, modal analysis, and experimental testing to determine its natural frequency. In all analytical approaches, the wing was modeled as a cantilever beam, with the root fixed and the tip free.

The structural analysis results were incorporated into the modal analysis system, where various mode shapes representing longitudinal deflections were identified. The first longitudinal mode shape, obtained through modal analysis, was observed at a frequency of 33.966 Hz, as illustrated in Figure 4.12. This mode shape features a single stationary node positioned near the fixed end of the structure, with the stationary regions highlighted in blue.

Additionally, modal frequencies were evaluated under different loading conditions. For the first longitudinal mode, the frequencies recorded under no-load and full-load conditions were 33.966 Hz and 21.617 Hz, respectively.

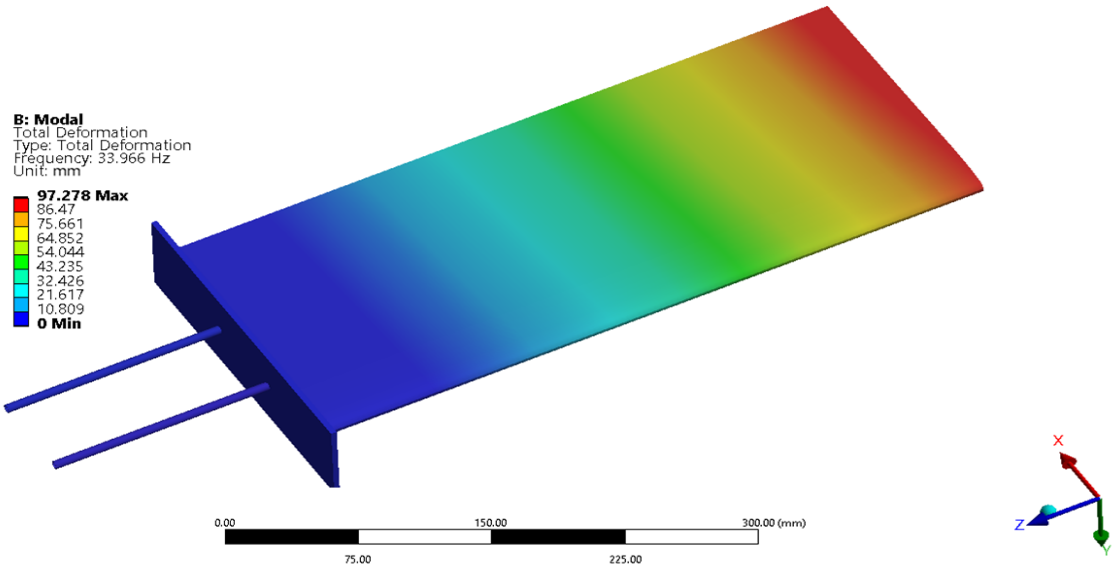

Figure 4.12: Contour of first longitudinal mode of vibration at no load condition

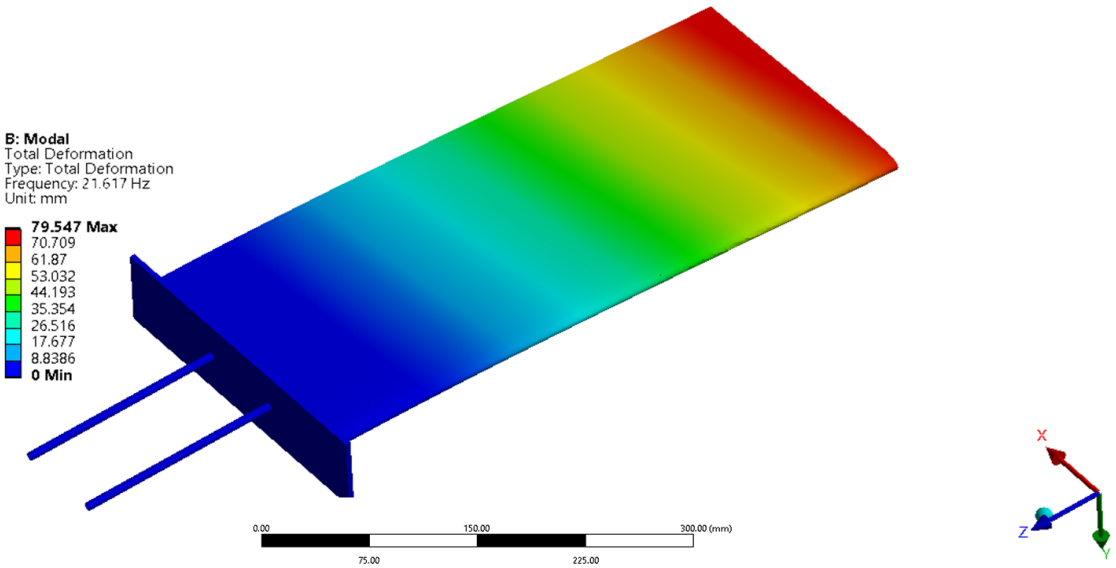

Figure 4.13: Contour of first longitudinal mode of vibration at full load condition

4.5. Estimation of Wing's Effective Young's Modulus

To estimate the effective Young's modulus of the wing, we applied the rule of mixtures, considering the different materials used in its construction. The wing consists of carbon fiber

skin and ribs (1.17 GPa) and a T300 carbon fiber tube spar (230 GPa). The total stiffness contribution was determined based on the volume fractions of these components within the wing's cross-section. While this estimation serves as a useful approximation for structural and vibration analysis, more precise methods such as finite element modeling or experimental validation would be required for an exact determination.

4.5.1. Calculating Young's Modulus Of Fabricated Carbon Fiber

In UTM, test specimen was put under test and maximum tensile strength was found to be 137 MPa. Deflection of 10.2 mm was found to be the elongation before failure of specimen. Though the result was obtained, the gripping of specimen wasn't satisfactory. This process can be done efficiently with adhesion of rubber pads.

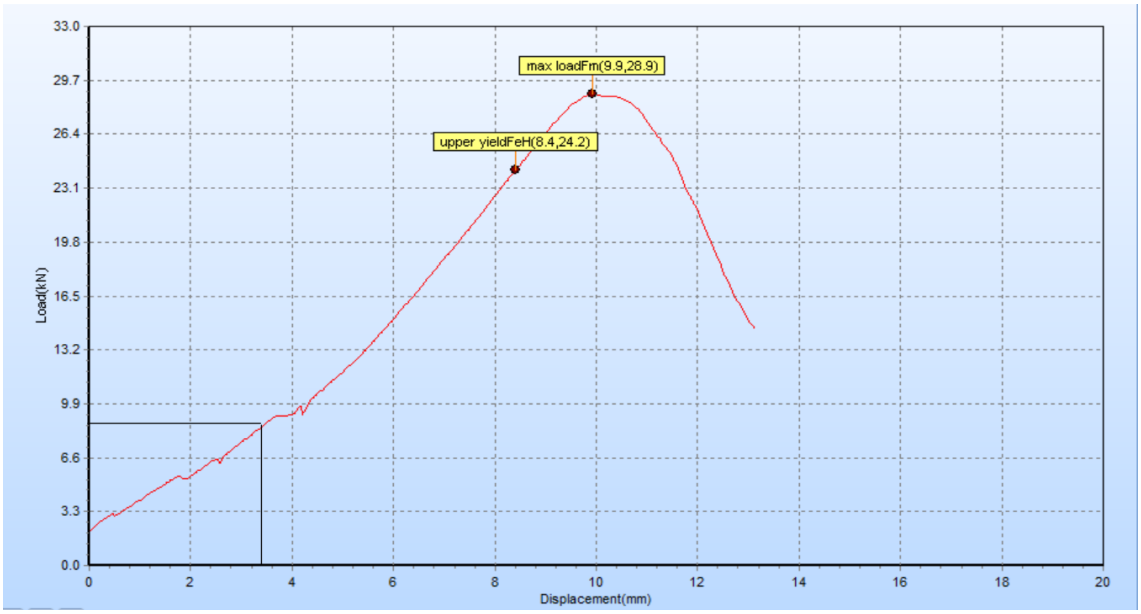

Figure 4.14: Experimental Load vs. Displacement graph from which stress and strain values were extracted for Young's modulus calculation

Parameter before test		
extensoment gauge[mm]	0.0	mm
area[mm^2]	210.00	mm^2
original gauge[mm]	81.88	mm
Thickness[ao]	7.00	mm
Width[bo]	30.00	mm
Parameter after test		
max load[kN]	28.9	kN
tensile strength[Mpa]	137.6	MPa
min area after fracture[mm]		mm^2
gauge after fracture[mm]	0.00	mm
elongation after fracture[mm]		mm
percentage elongation after fracture[A]		%
total elongation after fracture[mm]	0.00	mm
percentage total extension after fract...		%
yield[kN]	24.25	kN
yield strength[Mpa]	115.5	MPa
total extension load[kN]		kN
total extension strength[Rt]		MPa

Figure 4.15: Tensile Test Data for Determining Young's Modulus

Formula for Young's Modulus: Young's modulus (E) of a material can be calculated using the following formula:

$$E = \frac{\sigma}{\varepsilon} \tag{4.1}$$

where stress (σ) and strain (ε) are given by:

$$\sigma = \frac{F}{A} \tag{4.2}$$

$$\varepsilon = \frac{\Delta L}{L_0} \tag{4.3}$$

Data from the Image:

- Original Cross-sectional Area (A) = 210 mm^2
- Original Gauge Length (L_0) = 81.88 mm
- Load at the linear elastic region (before yield point) = 9 kN
- Displacement at the same load (ΔL) = 3 mm (approx.)

Stress Calculation:

$$\sigma = \frac{9000}{210} = 42.86 \times 10^6 \text{ Pa} = 42.86 \text{ MPa} \tag{4.4}$$

Strain Calculation:

$$\varepsilon = \frac{3}{81.88} = 0.0366 \tag{4.5}$$

Young's Modulus Calculation:

$$E = \frac{42.86 \text{ MPa}}{0.0366} = 1.17 \times 10^3 \text{ MPa} = 1.17 \text{ GPa} \tag{4.6}$$

Thus, the Young's modulus is approximately:

$$E \approx 1.17 \text{ GPa} \tag{4.7}$$

In this project, the tensile strength of the fabricated carbon fiber composite was evaluated to understand its mechanical behavior. Although carbon fiber is inherently anisotropic—exhibiting different properties in different directions—we assumed a quasi-isotropic behavior for our engineering application. This assumption was justified by the method we adopted during fabrication. By carefully controlling the orientation of the carbon fiber plies in the laminate, we achieved a balanced layup that allowed the composite to exhibit nearly uniform strength and stiffness within the plane. This quasi-isotropic approach simplifies analysis and design while still maintaining the benefits of carbon fiber, making it suitable for our wing structure where consistent in-plane properties are essential.

Carbon fiber specimen tested in the paper [31] shows result for Young's modulus (E) in different conditions. For the non reinforced and reinforced carbon fiber, the value for Young's modulus was found to be in between 0.419 to 20.233 GPa. Also the value of maximum tensile strength was cited as 44.5 to 427.3 MPa. The specimen tested in this project had maximum tensile strength of 137 MPa which shows the specimen laminated had considerable strength lying in this range.

4.5.2. Determination of the Wing's Overall Young's Modulus Using the Rule of Mixtures

Step 1: Calculation of Volume Fractions

Our wing consists of:

- Skin & ribs made of carbon fiber (1.17 GPa)
- Spar made of a T300 carbon fiber tube (230 GPa)
- Acrylic plate support (2.9 GPa)

Volume of the Spar (Hollow Cylinder) The cross-sectional area of the spar is:

$$A_{spar} = \pi(R_{outer}^2 - R_{inner}^2) \tag{4.8}$$

$$\text{Outer diameter} = 10 \text{ mm} \Rightarrow R_{outer} = 5 \text{ mm}$$
$$\text{Inner diameter} = 8.5 \text{ mm} \Rightarrow R_{inner} = 4.25 \text{ mm}$$

$$A_{spar} = \pi(5^2 - 4.25^2) = \pi(25 - 18.06) = \pi(6.94) \approx 21.8 \text{ mm}^2 \tag{4.9}$$

Volume:

$$V_{ct} = 21.8 \times 10^{-6} \times 0.6 \times 2 = 2.616 \times 10^{-5} \text{ m}^3 \tag{4.10}$$

Mass:

$$M_{ct} = V_{ct} \times \rho_{ct} = 2.616 \times 10^{-5} \times 1790 = 0.04682 \text{ kg} = 46.82 \text{ g} \tag{4.11}$$

Weight of Ribs and Spars:

$$M_{cf} = 0.272 - 0.04682 = 0.22518 \text{ kg} \tag{4.12}$$

Volume of Carbon Fiber:

$$V_{cf} = \frac{M_{cf}}{\rho_{cf}} = \frac{0.22518}{1790} = 1.2626 \times 10^{-4} \text{ m}^3 \tag{4.13}$$

$$V_{acry} = \frac{M_{acry}}{\rho_{acry}} = \frac{0.118}{1180} = 1 \times 10^{-4} \text{ m}^3 \tag{4.14}$$

Total Volume:

$$V_t = V_{cf} + V_{ct} + V_{acry} = 1.2626 \times 10^{-4} + 2.616 \times 10^{-5} + 10^{-4} = 2.5242 \times 10^{-4} \text{ m}^3 \tag{4.15}$$

$$E_{acry} = 2.9GPa$$

Volume Fractions:

$$(VF)_{cf} = \frac{V_{cf}}{V_t} = 0.5002$$
$$(VF)_{acry} = \frac{V_{acry}}{V_t} = 0.4031$$
$$(VF)_{ct} = 1 - V_{cf} - V_{acry} = 1 - 0.5002 - 0.4031 = 0.0967$$

Step 2: Apply the Rule of Mixtures

$$E_{wing} = E_{skin}(VF)_{cf} + E_{spar}(VF)_{ct} + E_{acry}(VF)_{acry} \tag{4.16}$$

$$E_{wing} = (1.17 \times 0.5002) + (230 \times 0.0967) + (2.9 \times 0.4031) \tag{4.17}$$

$$E_{wing} = 23.996 \text{ GPa} \tag{4.18}$$

Thus, the estimated Young's modulus of the wing is approximately 23.996 GPa, which provided a useful approximation for our vibration analysis.

Object	Young's Modulus (GPa)
$E_{specimen}$	1.17
E_{wing}	23.996
E_{cited}	0.419–20.233

Table 4.2: Comparison of Young's Modulus values

4.6. Analytical Solution for Wing Vibration Analysis

4.6.1. Structured Columns from the Clark Y Airfoil Profile Data

X (mm)	Upper Surfaces	Lower Surfaces	Differences	Averages
250	0.149825	-0.14983	0.29965	0
247.5	0.74225	-0.24165	0.9839	0.2503
245	1.333375	-0.33348	1.66685	0.49995
242.5	1.9217	-0.42528	2.346975	0.748213
240	2.5058	-0.51708	3.022875	0.994363
235	3.655975	-0.7007	4.356675	1.477638
230	4.7789	-0.88433	5.663225	1.947288
225	5.875625	-1.06795	6.943575	2.403838
220	6.947275	-1.25158	8.19885	2.84785
215	7.9935	-1.4352	9.4287	3.27915
210	9.0134	-1.61883	10.63223	3.697288
205	10.00613	-1.80245	11.80858	4.101838
200	10.9709	-1.98608	12.95698	4.492413
195	11.90703	-2.1697	14.07673	4.868663
190	12.81413	-2.35333	15.16745	5.2304
185	13.69188	-2.53695	16.22883	5.577463
180	14.53998	-2.72058	17.26055	5.9097
175	15.35823	-2.90423	18.26245	6.227
170	16.14608	-3.08788	19.23395	6.5291
165	16.90115	-3.27155	20.1727	6.8148
160	17.62055	-3.45518	21.07573	7.082688
155	18.30138	-3.63878	21.94015	7.3313
150	18.94083	-3.82233	22.76315	7.55925
145	19.53628	-4.0058	23.54208	7.765238
140	20.087	-4.1893	24.2763	7.94885
135	20.5928	-4.37285	24.96565	8.109975
130	21.05363	-4.55655	25.61018	8.248538
125	21.4693	-4.74048	26.20978	8.364413
120	21.8393	-4.92465	26.76395	8.457325
115	22.16068	-5.10883	27.2695	8.525925
110	22.42938	-5.2927	27.72208	8.568338
105	22.64143	-5.47605	28.11748	8.582688
100	22.7928	-5.65853	28.45133	8.567138
95	22.8803	-5.84015	28.72045	8.520075
90	22.90665	-6.02175	28.9284	8.44245

Continued on next page

X (mm)	Upper Surfaces	Lower Surfaces	Differences	Averages
85	22.87698	-6.2044	29.08138	8.336288
80	22.79643	-6.38913	29.18555	8.20365
75	22.6701	-6.57698	29.24708	8.046563
70	22.5004	-6.7674	29.2678	7.8665
65	22.271	-6.9541	29.2251	7.65845
60	21.9577	-7.12953	29.08723	7.414088
55	21.53583	-7.28613	28.82195	7.12485
50	20.98005	-7.4164	28.39645	6.781825
45	20.26718	-7.51225	27.77943	6.377463
40	19.39268	-7.56365	26.95633	5.914513
35	18.359	-7.5601	25.9191	5.39945
30	17.1551	-7.49083	24.64593	4.832138
25	15.74953	-7.34465	23.09418	4.202438
20	14.1077	-7.11488	21.22258	3.496413
15	12.18928	-6.78193	18.9712	2.703675
12.5	11.06883	-6.5113	17.58013	2.278763
10	9.782075	-6.13028	15.91235	1.8259
7.5	8.255375	-5.6514	13.90678	1.301988
5	6.343375	-5.06808	11.41145	0.63765
3	4.464525	-4.24333	8.70785	0.1106
2	3.43375	-3.57155	7.0053	-0.0689
1	2.23095	-2.62815	4.8591	-0.1986
0.5	1.450625	-1.95283	3.40345	-0.2511
0.25	0.931775	-1.48545	2.417225	-0.27684
0.125	0.58475	-1.1675	1.75225	-0.29138
		Maximum	**29.2678**	**8.582688**

Table 4.3: Measured values for the airfoil profile Clark Y

The maximum values found from the last two columns are:

- $t = 29.2678$ mm
- $h = 8.582688$ mm

From the design of the wing, we have:

- Chord length, $c = 0.25$ m
- Wing length, $L = 0.6$ m

For the selected material (Carbon Fiber), the properties used from calculations are:

- Young's modulus, $E = 23.206$ GPa
- Density, $\rho = 1790$ kg/m^3

4.6.2. Theoretical Calculation of Wing Vibrations

The Euler-Bernoulli equation from Eq. 2.1 is used to calculate the frequency of wing,

$$\omega_n = (\beta_n L)^2 \sqrt{\frac{EI}{mL^4}} \tag{4.19}$$

Using Eq. (2.9-2.14), the following results were obtained:

$$A = K_A ct = 0.86 \times 0.25 \times 29.2678 \times 10^{-3} = 6.293 \times 10^{-3} \tag{4.20}$$

$$I = K_{tct}(t^2 + h^2) = 0.036 \times ((29.2678 \times 10^{-3})^2 + (8.5826 \times 10^{-3})^2) = 2.45042 \times 10^{-7} m^4 \tag{4.21}$$

c (mm)	t (mm)	h (mm)	T	ε	L (mm)	A (mm^2)
250	29.2678	8.582688	0.117071	0.034331	600	6293

Table 4.4: Computed parameters for the airfoil wing

The natural angular frequency was found after substituting all the known parameters:

$$m = \rho \times A = 1790 \times 6.293 \times 10^{-3} = 11.264 kg/m \tag{4.22}$$

$$\omega_n = (\beta_n L)^2 \sqrt{\frac{(23.996 \times 10^9) \times (2.45042 \times 10^{-7})}{11.264 \times (0.6)^4}} \tag{4.23}$$

$$\omega_n = (\beta_n L)^2 = 1.875^2 \times 63.466 = 223.123 \text{ rad/s}$$

The frequency in Hz is:

$$f = \frac{223.123}{2\pi} = 35.51 \text{ Hz}$$

4.7. Wing Prototype Fabrication

A systematic design and manufacturing process was implemented using SolidWorks to refine the wing prototype, ensuring standardization and structural optimization. Two different materials, carbon fiber and glass fiber, were evaluated through simultaneous testing, ultimately leading to the selection of carbon fiber due to its superior strength-to-weight ratio and easiness in layup process.

For the rib sections, two layers of carbon fiber cloth were combined with resin and hardener, followed by UV curing to enhance structural integrity. The cured composite was then precisely cut into the required rib shapes using a grinder cutting machine, guided by 3D-printed rib profiles.

The spars were constructed using two 8.5mm cylindrical carbon rods, providing the necessary rigidity. A single-layer carbon fiber skin was fabricated through the hand layup process and cured under bright sunlight to achieve the desired strength.

Finally, the assembly of the internal structure, including ribs and spars, was carried out using epoxy and hardener for secure attachment. The wing skin was then affixed to the assembled structure using a high-strength adhesive, ensuring a durable and aerodynamically efficient final product.

4.8. Test rig setup for Vibrational Analysis

To validate the structural performance of the wing, XFLR5 software was used to analyze aerodynamic forces. At an AOA of 5° and a wind speed of 15 m/s, the lift force acting on the wing was computed as 15.29 N. The drag force was 0.32 N, leading to net usable lift of 14.97 N.

For structural load assessment, the wing was modeled as a cantilever beam with a fixed root and a free tip. The half-wing load was determined to be 14.97 N, and applying an ultimate

load factor of 1.5, the maximum load capacity of the wing was calculated as:

$$\text{Ultimate Load} = 14.97 \times 1.5 = 22.45 \text{ N}$$

This analysis ensures that the wing design meets structural safety requirements under aerodynamic loading conditions.

Figure 4.16: Experimental setup for capturing motion using high speed camera

4.9. Evaluation of Experimental Results

4.9.1. Empirical Modal Assessment

The experimental structural testing utilized digital motion capture analysis, offering significant advantages in efficiency, versatility, and accessibility over traditional transducer-based measurement methods. A Chronos 1.4 high-speed camera was employed to record motion at 1000 fps, ensuring the capture of high-resolution frames essential for analysis. The recorded frames were then processed in MATLAB to generate a Fast Fourier Transform (FFT) plot, representing the Power Spectral Density (PSD) as a function of frequency.

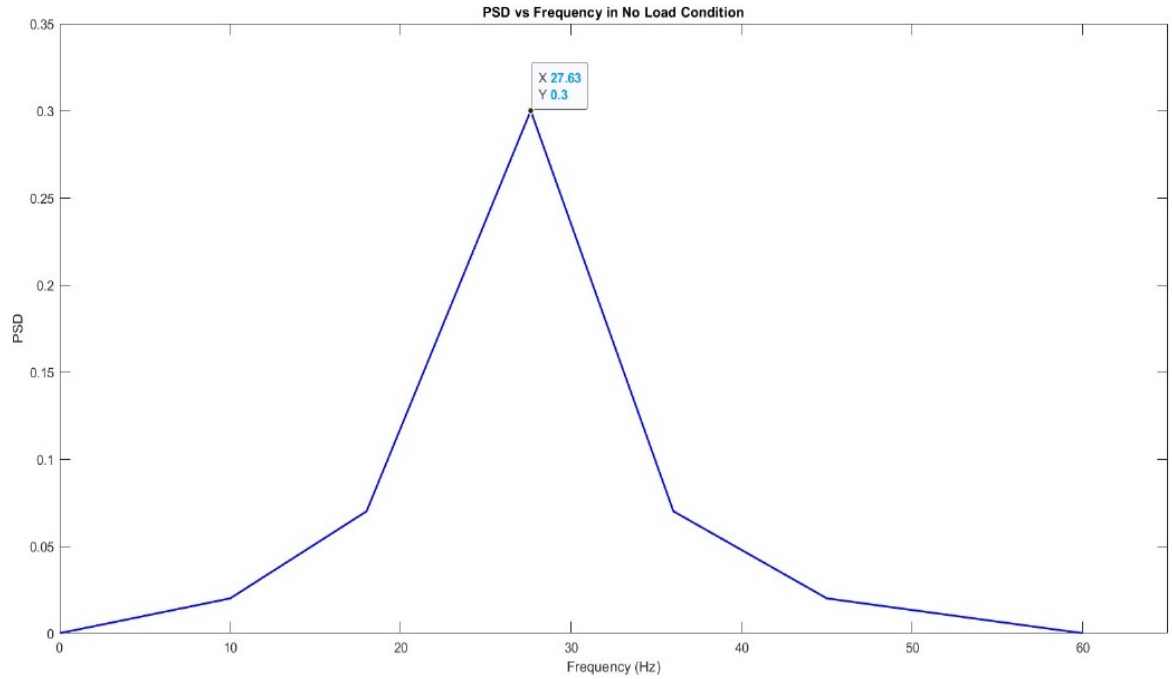

Figure 4.17: FFT plot illustrating the Power Spectral Density (PSD) as a function of frequency under no-load conditions.

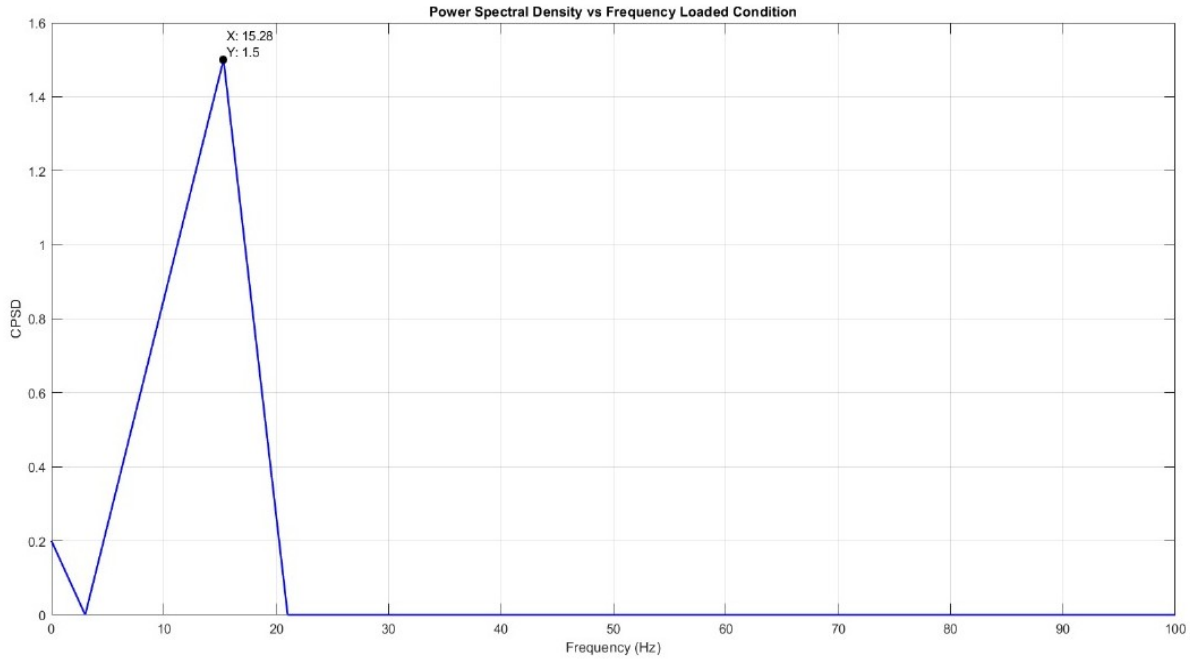

Figure 4.18: FFT plot illustrating the Power Spectral Density (PSD) as a function of frequency under full load conditions.

The peaks observed in the FFT plot represent distinct frequencies at which the wing structure undergoes significant vibrational modes. These peaks are critical for precisely identifying

the natural frequencies of the structure, as they highlight the resonant frequencies where the wing exhibits maximum deflection or vibration. By analyzing these frequencies, we can gain valuable insights into the dynamic behavior of the wing and its response to different loading conditions.

Under no-load conditions, the natural frequency of the wing was found to be 27.63 Hz, while under full load, it decreased to 15.28 Hz, as shown in Figures 4.16 and 4.17. This decrease in frequency as the load increases is consistent with expectations, as the natural frequency is inversely related to the structural stiffness and mass. As the load on the wing increases, the structure becomes more flexible, leading to a reduction in stiffness and, consequently, a lower natural frequency. Additionally, as more mass is added to the structure due to the load, the natural frequency further decreases, as predicted by the natural frequency equation:

The natural frequency f is given by:

$$f = \frac{1}{2\pi}\sqrt{\frac{k}{m}}$$

Where:

- f is the natural frequency,
- k is the stiffness of the structure, and
- m is the mass of the structure.

The observed decrease in frequency aligns with this theoretical understanding, confirming that both the increased load and added mass contribute to the structural flexibility of the wing. This behavior is crucial for the design and optimization of UAV wing structures, as it highlights the importance of considering load effects in the dynamic performance of the wing.

4.9.2. Wind Tunnel Analysis Results

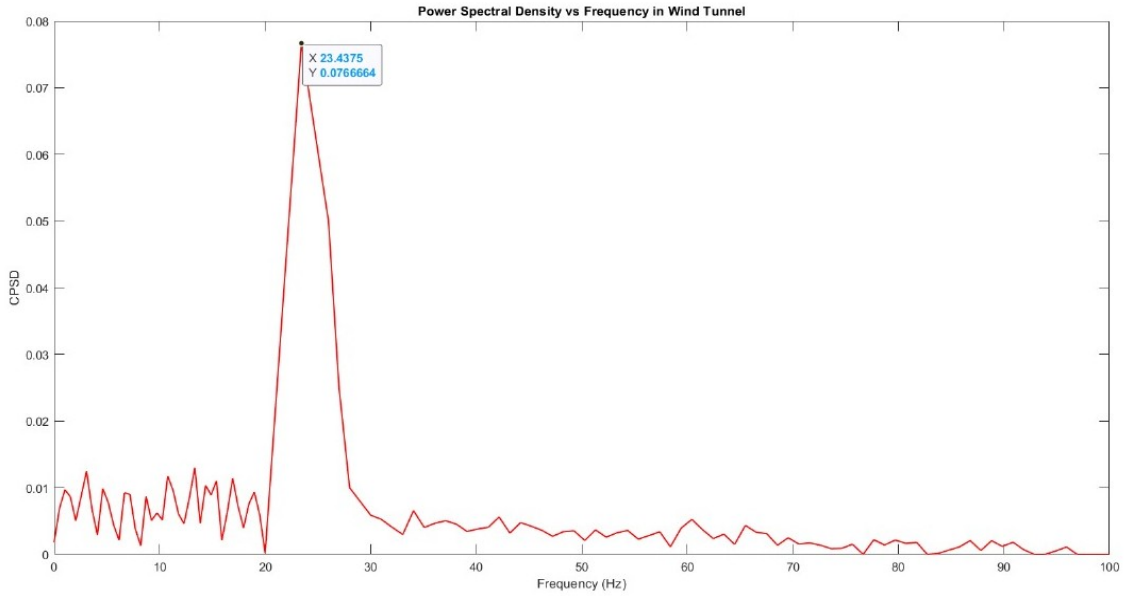

Figure 4.19: FFT plot illustrating the Power Spectral Density (PSD) as a function of frequency under (at 8.62 m/s)

For the vibrational motion analysis of the wing, an open jet fan array subsonic wind tunnel was utilized, with an airflow velocity of 8.62 m/s. High-speed cameras were employed to capture visual TIFF data during the wind tunnel test, which was subsequently processed and analyzed using MATLAB. The frequency obtained from the data analysis was 23.4375 Hz, as illustrated in Figure 4.18. This value closely matched the frequency of 27.23 Hz observed under the no-load condition during experimental modal analysis. The slight difference between the two frequencies could be attributed to the differences in loading conditions and the aerodynamic effects experienced during wind tunnel testing. This reinforces the reliability of the experimental modal analysis while demonstrating the practicality and consistency of wind tunnel testing for assessing vibrational behavior.

4.9.3. Damping Ratio Analysis:

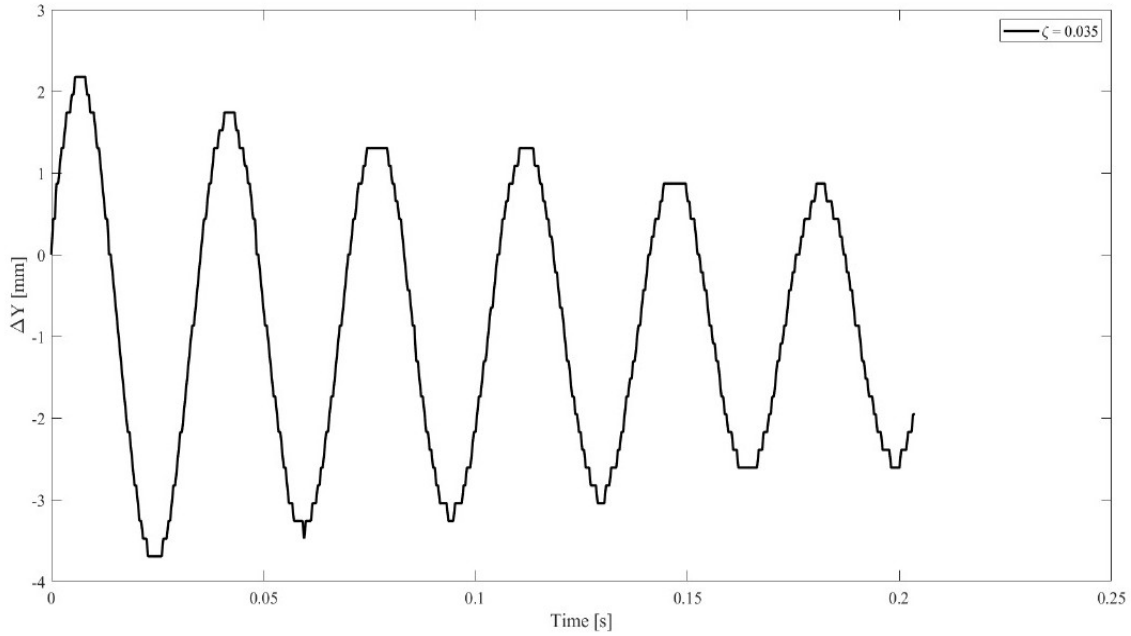

Figure 4.20: Damping curves for the peaks and troughs of the deformation signal under the no-load condition.

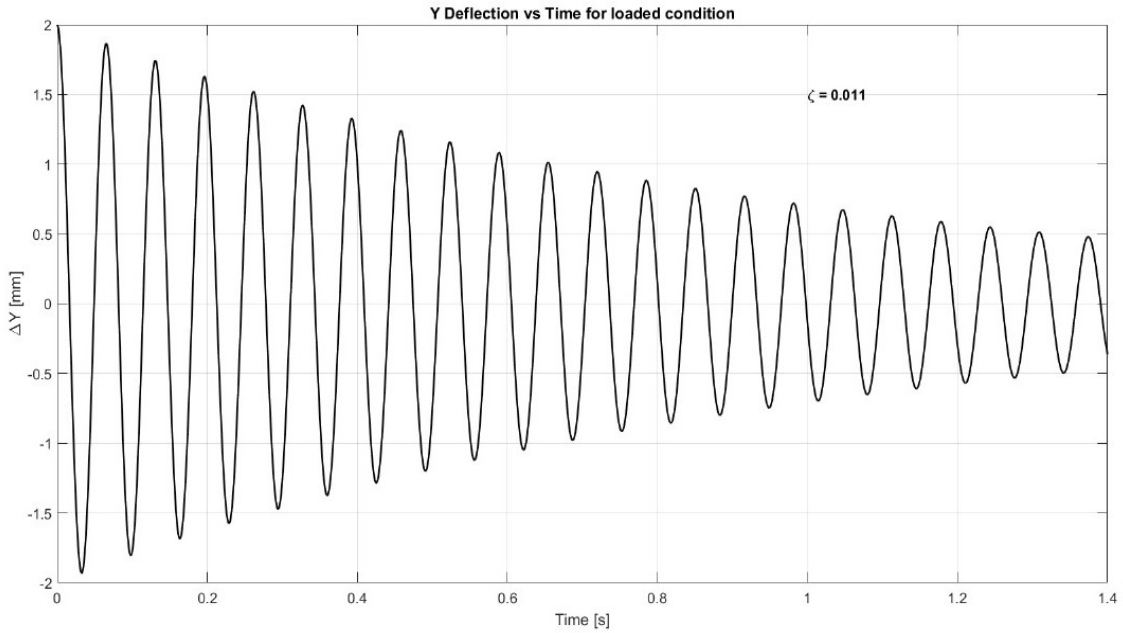

Figure 4.21: Damping curves for the peaks and troughs of the deformation signal under the full load condition.

The damping ratio decreases as the system transitions from the no-load condition to the loaded condition. The mean damping ratio values for the peaks and troughs of the displacement curves are shown in the legend sections of Figures 4.20 and 4.21. A lower damping ratio, closer to 0, signifies a more oscillatory, underdamped response, indicating that the wing structure exhibits more pronounced oscillations under load. In contrast, a higher damping ratio, approaching 1, implies a faster, critically damped response, where oscillations decay more rapidly.

The results suggest that when the wing is subjected to aerodynamic loading, it becomes less effective at dissipating energy (lower real part) and more susceptible to oscillations or vibrations (higher imaginary part) compared to the no-load condition. This change in damping behavior has significant implications for the structural response, as it affects the dynamic stability, resilience to external forces, and overall performance of the wing under varying loading conditions.

4.9.4. Comparison of Analytical, Experimental, and Simulated Frequencies

In this section, the obtained natural frequencies from three different approaches—analytical calculations, experimental testing, and numerical simulations—are compared. The analytical method provides a theoretical estimate based on mathematical modeling, while the experimental results were obtained through physical testing. The simulated frequency was derived using computational methods. The comparison highlights the deviations between these methods, which can be attributed to factors such as material properties, boundary conditions, and experimental limitations.

S.N.	Method	Fequency
1	Analytical	35.51Hz
2	Experimental	27.63Hz
3	Simulations	33.69Hz

Table 4.5: Comparison of Analytical, Experimental, and Simulated Frequencies

To assess the relationship between these results, we calculated the percentage deviation of experimental and simulation values from the analytical value:

- **Experimental Deviation from Analytical:**

$$\frac{35.51 - 27.63}{35.51} \times 100 = 22.19\%$$

- **Simulation Deviation from Analytical:**

$$\frac{35.51 - 33.69}{35.51} \times 100 = 5.12\%$$

- **Experimental Deviation from Simulation:**

$$\frac{33.69 - 27.63}{33.69} \times 100 = 17.98\%$$

The results indicate that the analytical and simulation values are closely aligned, with a deviation of 5.12%, suggesting that the assumptions in the simulation closely resemble the theoretical model. However, the experimental value shows a 22.19% deviation from the analytical result, which can be attributed to factors such as material imperfections, fabrication inconsistencies, and boundary conditions not perfectly replicated in real-world testing. The deviation of 17.98% between the experimental and simulation results further highlights the challenges in achieving an ideal experimental setup. These variations emphasize the need for precise fabrication, improved curing methods, and more controlled testing conditions to reduce discrepancies in future studies.

4.9.5. Microscopic Study of Cured Surface

Leica DM750 digital microscope was used to observe the cure surfaces. The surfaces were seen at 5x zoom. The study of cured surface is critical for the study of strength of the final product.

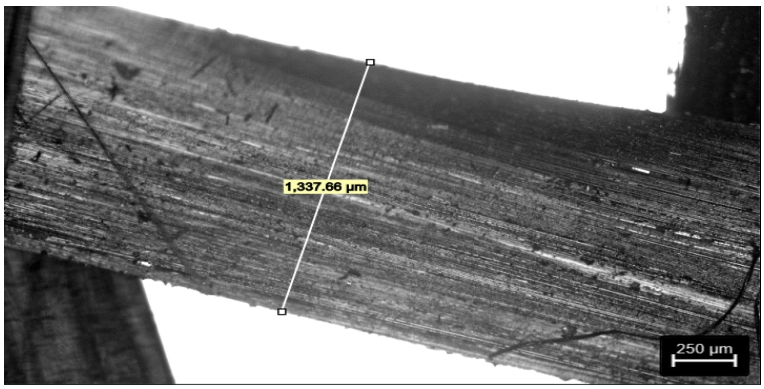

Figure 4.22: Fiber thread measurement though microscope

Above figure shows the fiber thread length measured through microscope. Length of fiber was found to be 1337.66 µm.

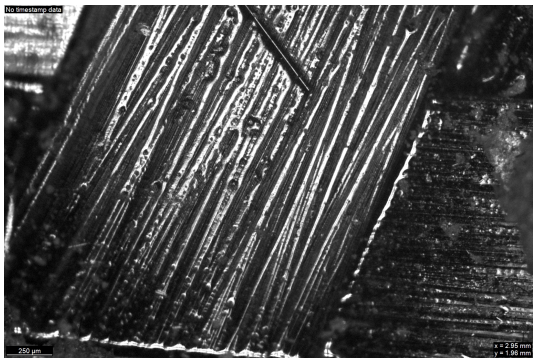

Figure 4.23: Uneven distribution of resin

Figure 4.24: Smooth surface finish after resin curing

Through the microscope we observed the distribution of resin. The distribution wasn't smooth for all the sections. The reasons for this could be due to:

- Overuse of resin on the surface than required.
- Improper use of brush and roller while applying.
- Flow of resin while curing as vacuum bagging wasn't performed.

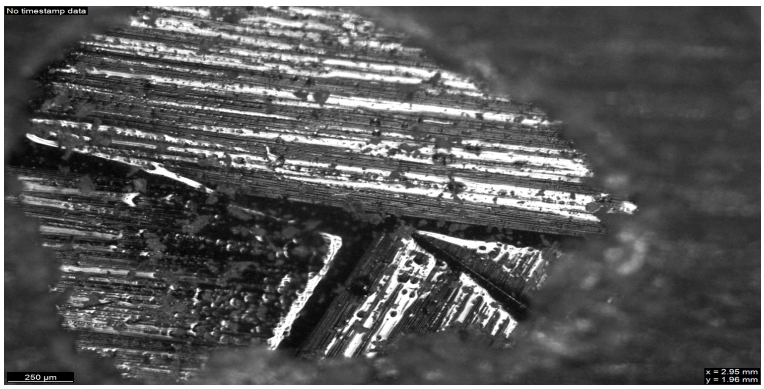

Figure 4.25: Hole in resin layer due to interference during curing

Another problem that might occur during curing is he movement of the fibre cloth during curing. Or external disturbances might occur. The hole shown in the Fig.4.25 is due to the presence of foreign substance during curing which was later removed. This reduces the strength of the section as the fibre cloth is exposed directly without layer of resin.

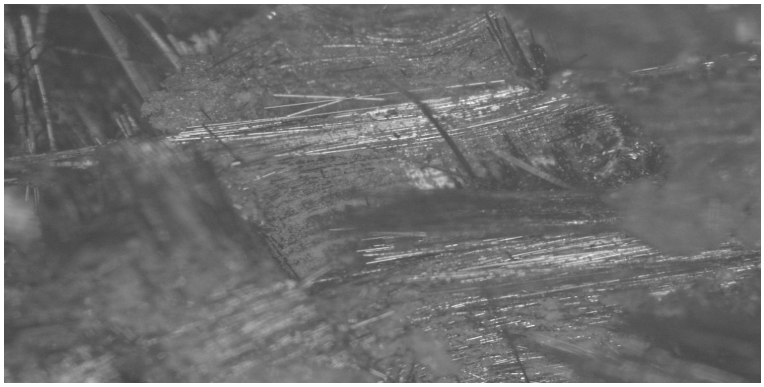

Figure 4.26: Fibres after the breakage of test specimen

The tested specimen in UTM was also put under observation. It was found from the image that the thread disintegrated into finer pieces after breaking. As our specimen was brittle, there was sudden breakage. The disintegrated fibres could also be seen to have brittle shapes at the ends.

This part of the project could be continued and studied better in future for the material property evaluation in different cases.

4.10. Limitations

i. The analysis in this study is limited to the first mode of longitudinal vibration, without consideration of higher vibration modes.

ii. The wing was fabricated using the hand-layup process without the use of a vacuum pump or a temperature-controlled environment for curing.

iii. The study does not account for potential bias in the impact hammer measurements during vibration analysis.

4.11. Problems Faced

During the project, several challenges were encountered that affected the overall process and results. The curing process was conducted without a temperature-controlled environment, leading to suboptimal curing due to low temperatures. While a UV curing setup was available, its limited size made it unsuitable for developing a wing. Additionally, resin storage posed difficulties, as low temperatures made it hard to stir and mix properly. During testing in the Universal Testing Machine (UTM), the grip of the test specimen was inadequate to fully support the applied load. Furthermore, the UTM required a minimum specimen thickness of 5mm, which demanded a larger amount of fiber cloth. Achieving precise cuts on cured fiber cloth using a laser and hand grinder was also challenging, as the accuracy did not meet the required standards. Experimental validation for higher frequency modes proved difficult, and manufacturing constraints, along with the unavailability of additional test specimens, limited the development of more samples. Moreover, noticeable differences were observed between simulation results and experimental findings, adding complexity to the analysis.

4.12. Safety and Precautions

i. Always use PPE (Personal Protective Equipments) for safety of your own.

ii. Use mask if there is need for cutting of fiber parts or if heat is to be applied to fiber.

iii. Cover every body part while working with cured glass fiber as it might cause sensation of cut and burning if contacted with skin.

iv. Use gloves while using chemicals as they might stick to skin or are harmful generally.

v. Dispose resin properly if there is any left after completion of work.

vi. Always remember to use releasing wax before applying resin to any surface.

vii. In case of resin getting attached to surface, acetone might be used to remove adhesion. It has to be done with utmost care as acetone is highly flammable and might cause damage to structure.

4.13. Work Schedule

S.N.	Work	Time Frame
1	Literature Review	9 Months
2	Proposal Writing	3 Weeks
3	Industrial Visit	10 Times
4	Wing Design	4 Weeks
5	Applying different Molding techniques	8 Weeks
6	Fabrication of test specimen and UTM testing	3 Weeks
7	Simulations	6 Weeks
8	Mid Term Report Preparation	4 Weeks
9	Fabrication and assembly of Wing	4 Weeks
10	Study of Analytical techniques to compute wing vibration	1 Week
11	Experimental Setup	2 Weeks
12	Data extraction using MATLAB	1 Week
13	Analysis of Result	2 Weeks
14	Final Report Preparation	4 Weeks

Table 4.6: Work Schedule Table

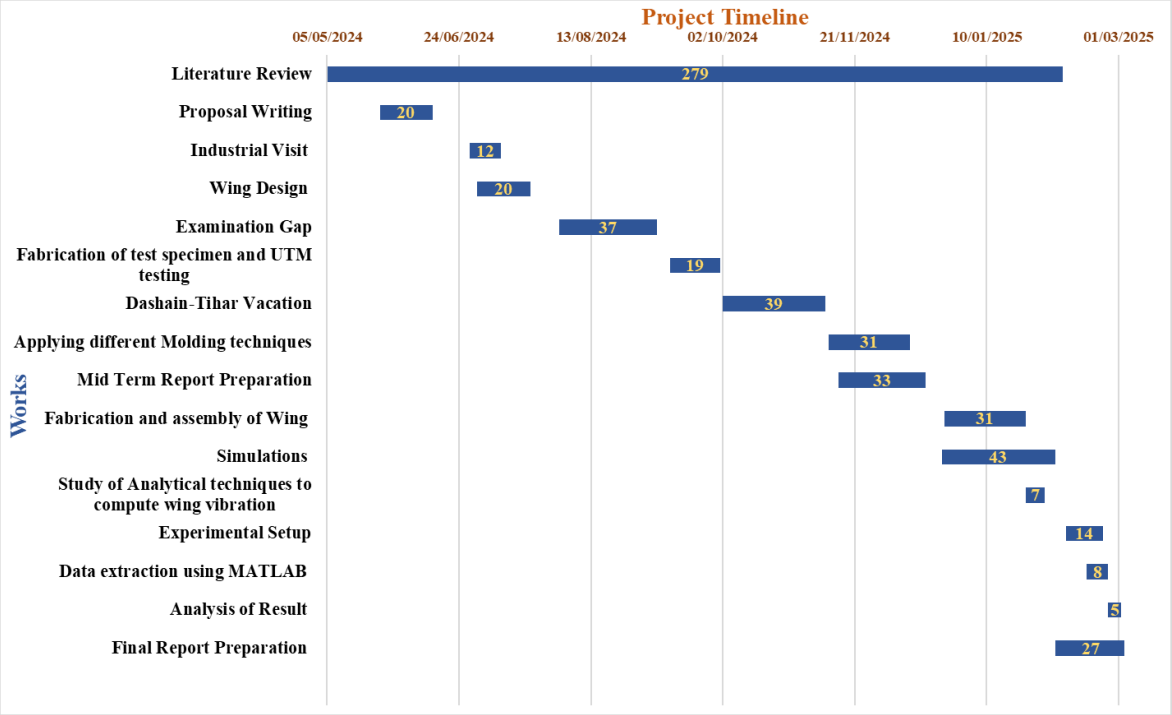

Figure 4.27: Gantt Chart

4.14. Budget Analysis

S.N.	Material	Cost
1.	Carbon Fiber Kit	10000
2.	3D Printing	6000
3.	Silicon and other molds	12000
4.	UV LED Lamp	5000
5.	Wood cutting cnc	3000
6.	Miscellaneous	5000
	Total	Rs.41000

Table 4.7: Budget Analysis

5. CONCLUSIONS AND RECOMMENDATIONS

5.1. Conclusion

This study on the fabrication, structural integrity, and dynamic response of a carbon fiber wing provides a comprehensive understanding of the material strength, resonance behavior, and overall performance of composite wing structures for UAV applications. The primary focus of the research was to investigate the impact of loading conditions on the wing's vibrational characteristics, including natural frequency and damping behavior, using analytical, numerical, and experimental methods. Carbon fiber, chosen for its superior strength-to-weight ratio, was successfully utilized in the fabrication of the wing through a hand layup process, ensuring both high structural integrity and lightweight properties.

The dynamic response of the wing was studied using modal analysis, wind tunnel testing, and experimental modal testing with high-speed motion capture. The results from both modal analysis, numerical analysis, and experimental testing were found to be in close agreement, reinforcing the reliability of the design and analysis process. A notable observation was the decrease in natural frequency with increasing load, highlighting the wing's greater flexibility under load and its susceptibility to dynamic resonance. Damping ratio analysis further illustrated that the wing exhibited more oscillatory behavior at loaded conditions, indicating a more underdamped response compared to the no-load condition. These findings suggest that as aerodynamic loading increases, the wing becomes less efficient at dissipating energy, thereby increasing the risk of flutter under heavy loading.

Ultimately, this research confirms that the carbon fiber wing, with its optimized design and fabrication process, exhibits commendable structural integrity and dynamic performance. The decrease in natural frequency under loading conditions, along with the variations in damping ratio, provides valuable insights into the resilience and dynamic stability of the wing. These results not only validate the use of carbon fiber composites for UAV wing applications but also underscore the importance of considering both material properties and loading conditions when designing lightweight, high-performance components. The successful development and testing of this UAV wing set a solid foundation for future advancements in UAV structural design and dynamic analysis, offering a pathway for further exploration and innovation in the field of unmanned aerial vehicles.

5.2. Recommendation

i. Study of different proportions of carbon fiber materials can provide valuable insights into how variations in fiber content affect the overall mechanical properties, such as strength, stiffness, and durability.

ii. Further study of material property especially microstructural properties could be studied in different cases. This could be done through testing material in different parameters of heat, pressure and so on.

iii. The use of an appropriately powered motor-driven vacuum pump is critical for maintaining consistent vacuum levels during fabrication.

iv. Further investigation into the higher modes of vibration and their correlation with both experimental and simulation results will provide deeper insights into the accuracy of the analysis. This can help identify potential resonance phenomena and critical frequency points that may affect the structural stability of the wing.

v. Correlating results from the modal analysis setup with data obtained from wind tunnel tests under varying conditions will allow for the validation and cross-checking of experimental data. This will help to identify any discrepancies and refine the understanding of the wing's dynamic behavior, ultimately improving the reliability of the design process.

References

[1] G. Agarwal, A. Patnaik, and R. Sharma, "Mechanical and thermo–mechanical properties of bi-directional and short carbon fiber reinforced epoxy composites," *Journal of Engineering Science and Technology*, vol. 9, no. 5, pp. 590–604, 2014.

[2] Z. Mostakim, N. Mehfuz, M. Zabal, K. A. Sajib, and M. Z. Hossain, "Comparison of vibration analysis among naca airfoil wings based on natural frequencies," in *International Conference on Mechanical, Industrial and Energy Engineering, December*, 2020, pp. 19–21.

[3] S. S. Rao, *Vibration of continuous systems*. John Wiley & Sons, 2019.

[4] D. Ozkan, M. S. Gok, and A. C. Karaoglanli, "Carbon fiber reinforced polymer (cfrp) composite materials, their characteristic properties, industrial application areas and their machinability," *Engineering Design Applications III: Structures, Materials and Processes*, pp. 235–253, 2020.

[5] P. Dharmendra, K. Chaithanya, A. Sameera, K. Kavathiya, and K. Monika, "Design and analysis of an aircraft wing rib for different configurations," *International Research Journal of Engineering and Technology*, vol. 7, no. 6, 2020.

[6] Y. Li, "The development of carbon fiber epoxy resin composite material and its applications in aerospace," *Applied and Computational Engineering*, vol. 23, pp. 75–80, 2023.

[7] H. Rahmani, S. H. M. Najafi, S. Saffarzadeh-Matin, and A. Ashori, "Mechanical properties of carbon fiber/epoxy composites: Effects of number of plies, fiber contents, and angle-ply layers," *Polymer Engineering & Science*, vol. 54, no. 11, pp. 2676–2682, 2014.

[8] Z. Yu, R. Li, Z. Peng, and Y. Tang, "Carbon fiber reinforced epoxy resin matrix composites," *Materials Science: Advanced Composite Materials*, vol. 1, no. 1, pp. 1–6, 2017.

[9] K. K. Agarwal and G. Agarwal, "A study of mechanical properties of epoxy resin in presence of different hardeners," *Technol. Innov. Mech. Eng*, pp. 1–9, 2019.

[10] S. Sulaiman, R. Yunus, N. Ibrahim, and F. Rezaei, "Effect of hardener on mechanical properties of carbon fibre reinforced phenolic resin composites," *Journal of Engineering Science and Technology*, vol. 3, no. 1, pp. 79–86, 2008.

[11] F. O. Abasi and R. U. Aabass, "Thermo-mechanical behavior of epoxy composite reinforced by carbon and kevlar fiber," in *MATEC web of Conferences*, vol. 225. EDP Sciences, 2018, p. 01022.

[12] G. Sanjuan, M. J. Lis Arias, J. Li, P. F. Coldea, C. López, J. Fernandez Vela, and G. Ruffini, "Go/rgo as reinforcing nanofiller in carbon fiber/epoxy resin composite systems," *Nanomaterial Chemistry and Technology*, vol. 1, no. 1, pp. 11–18, 2019.

[13] L. Markovičová, V. Zatkalíková, and P. Hanusová, "Carbon fiber polymer composites," in *Conference quality production improvement–CQPI*, vol. 1, no. 1, 2019, pp. 276–280.

[14] J. W. Hearle, *High-performance fibres*. Elsevier, 2001.

[15] B. Quinn, "Textile futures fashion design and technology," 2010.

[16] P. Morgan, "Carbon fibers and their composites," 2005.

[17] C. Riccardelli, "Carbon fiber fabric and its potential for use in objects conservation," *Objects specialty group postprints*, vol. 24, pp. 147–67, 2017.

[18] G. Özçakır, "Carbon fiber and its composites: Synthesis, properties, applications," *Sinop Üniversitesi Fen Bilimleri Dergisi*, vol. 9, no. 1, pp. 240–265, 2024.

[19] V. Shukla, M. Bajpai, D. Singh, M. Singh, and R. Shukla, "Review of basic chemistry of uv-curing technology," *Pigment & Resin Technology*, vol. 33, no. 5, pp. 272–279, 2004.

[20] A. Endruweit, M. Johnson, and A. Long, "Curing of composite components by ultraviolet radiation: A review," *Polymer composites*, vol. 27, no. 2, pp. 119–128, 2006.

[21] N. Kuntoji and V. Kuppast, "Study of aircraft wing with emphasis on vibration characteristics," *International Journal of Engineering Research and Application*, vol. 7, no. 4, pp. 1–8, 2017.

[22] E. Carrera, M. Petrolo, and A. Varello, "Advanced beam formulations for free-vibration analysis of conventional and joined wings," *Journal of Aerospace Engineering*, vol. 25, no. 2, pp. 282–293, 2012.

[23] A. Demirtaş and M. Bayraktar, "Free vibration analysis of an aircraft wing by considering as a cantilever beam," *Selçuk Üniversitesi Mühendislik, Bilim Ve Teknoloji Dergisi*, vol. 7, no. 1, pp. 12–21, 2019.

[24] J. Najmi, H. A. Khan, S. S. Javaid, A. Hameed, and F. Siddiqui, "Aeroelastic tailoring for aerospace applications," *Heliyon*, vol. 10, no. 2, 2024.

[25] W. C. Young, R. G. Budynas, and R. J. Roark, *[Formulas for stress and strain]; Roark's formulas for stress and strain*. McGraw-Hill, 2002.

[26] K. Z. Yang and I. D. I. F. Nusyirwan, "Design of a small unmanned aircraft," *Science and Engineering*, vol. 3, 2015.

[27] P. SHIVA, G. D. SINGH, R. KUKAL, and S. KUMAR, "Design and fabrication of wing of a high-payload aerial vehicle."

[28] S. Sharma, U. Sharieff, A. Singh, and R. Tarnacha, "Design and fabrication of fixed-wing uav for commercial monitoring," *Int. J. Eng. Res. Technol*, vol. 8, pp. 1153–1177, 2021.

[29] L. P. P. S. P. Abhishek Bhandari, Sudip Bhattarai, "Design, fabrication and structural analysis of a uav wing employing modern materials and manufacturing methods," *IOE Graduate Conference*, 2023.

[30] S. K. Das and S. Roy, "Finite element analysis of aircraft wing using carbon fiber reinforced polymer and glass fiber reinforced polymer." in *IOP conference series: Materials science and engineering*, vol. 402, no. 1. IOP Publishing, 2018, p. 012077.

[31] B. Nowinka and D. Sykutera, "Mechanical properties of carbon fiber reinforced polyamide produced by cff method (continuous filament fabrication)," in *MATEC Web of Conferences*, vol. 332. EDP Sciences, 2021, p. 01006.

A. APPENDIX 1: Fabrication Process

Figure A.1: Carbon Fiber layup process using wood mold

Figure A.2: Resin to Hardener mix weight measurement (100:40)

Figure A.3: Cured carbon fiber wing skin shaped using a wooden mold

Figure A.4: Assembly of wing internal structure

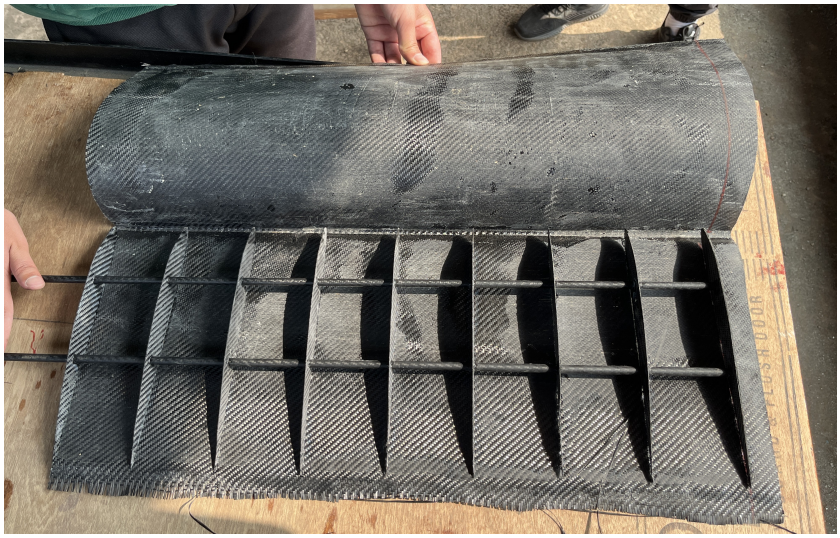

Figure A.5: Skin internal structure integration process

Figure A.6: Grinding off the surplus wing skin material.

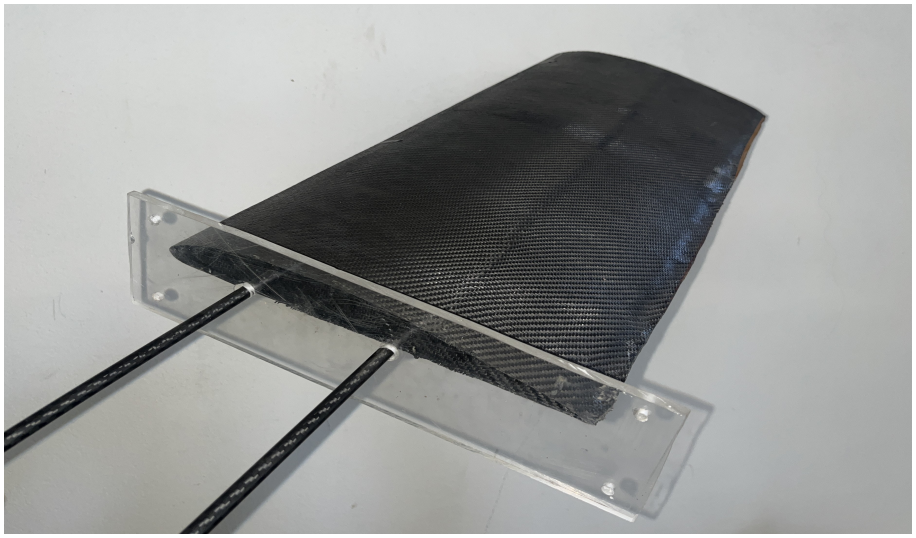

Figure A.7: Final assembled wing

Figure A.8: Total Weight measurement of assembled wing

B. APPENDIX 2: Experimental setups

Figure B.1: Microscope setup for analyzing fiber diameter and resin-hardener distribution in the composite layup.

Figure B.2: Vibrational analysis data collection setup

Figure B.3: Wind Velocity measurement in wind tunnel

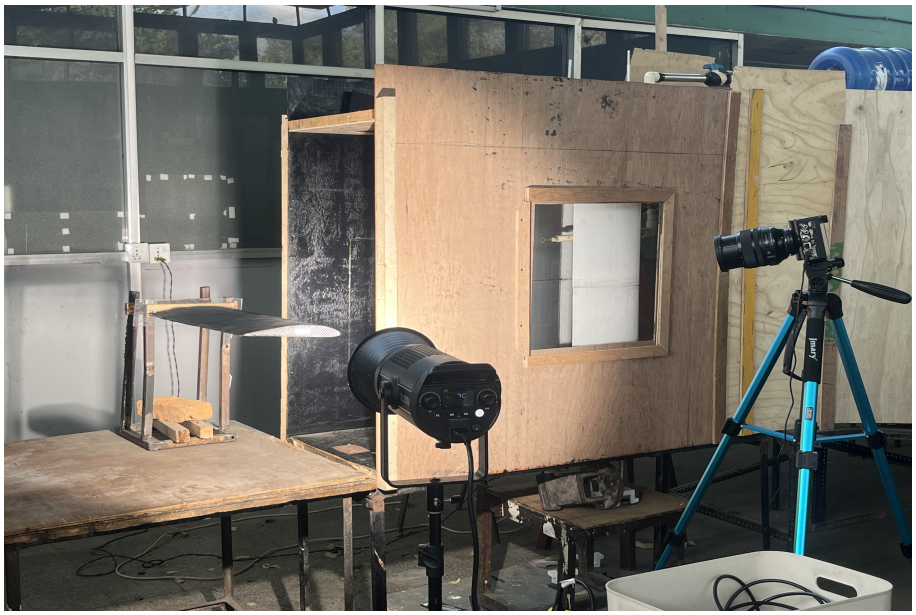

Figure B.4: Wind tunnel vibration capturing Setup with proper lightening.

C. APPENDIX 3: Results from software

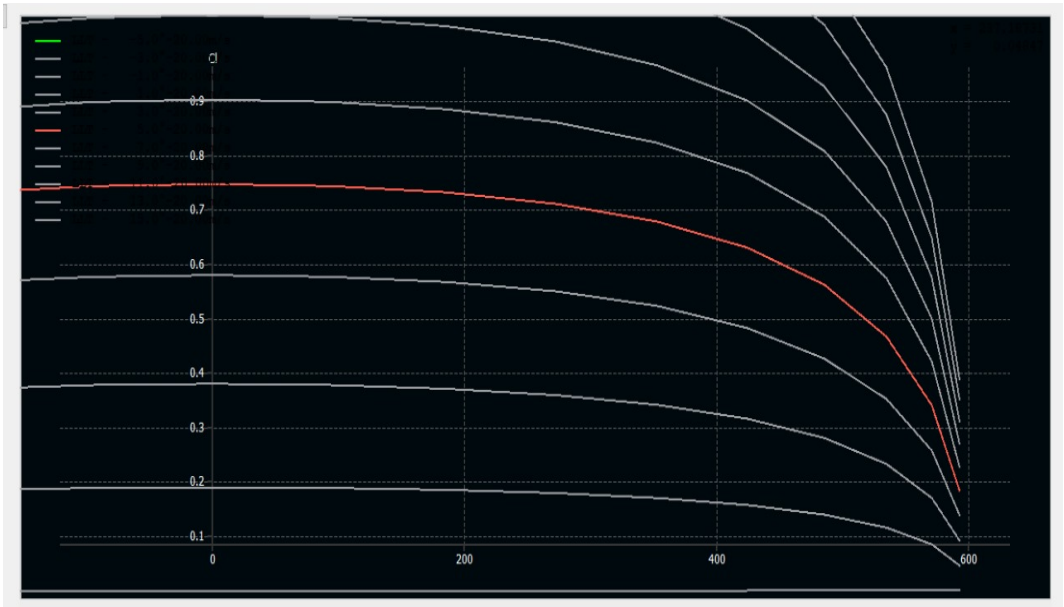

Figure C.1: Lift coefficient (Cl) variation along the wingspan, generated using XFLR analysis.

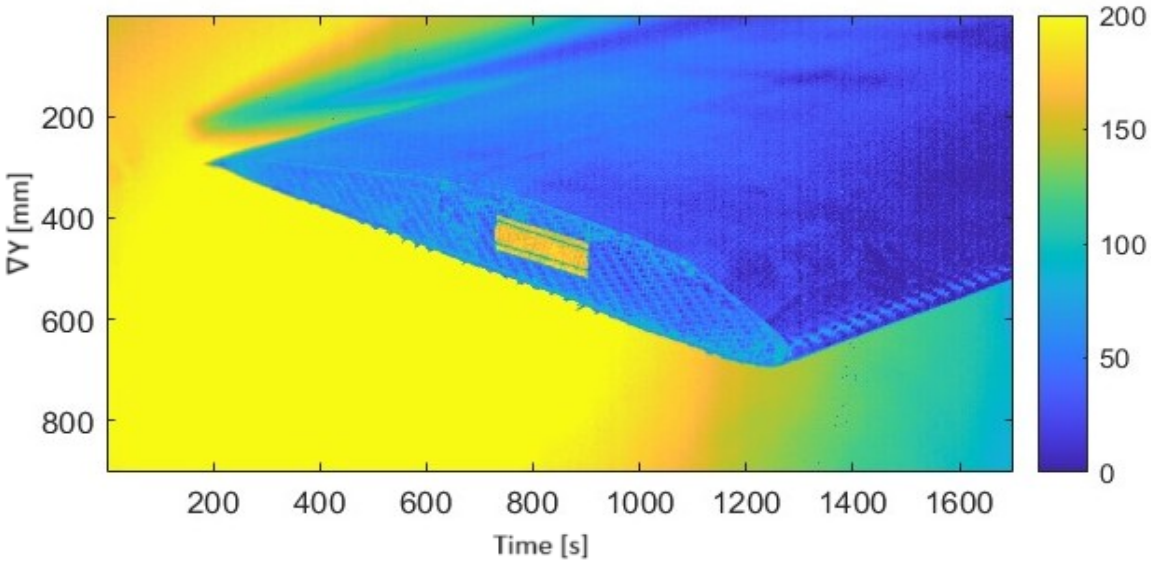

Figure C.2: MATLAB image processing